



AFTAC

Air Force Technical Applications Center

Directorate of Nuclear Treaty Monitoring

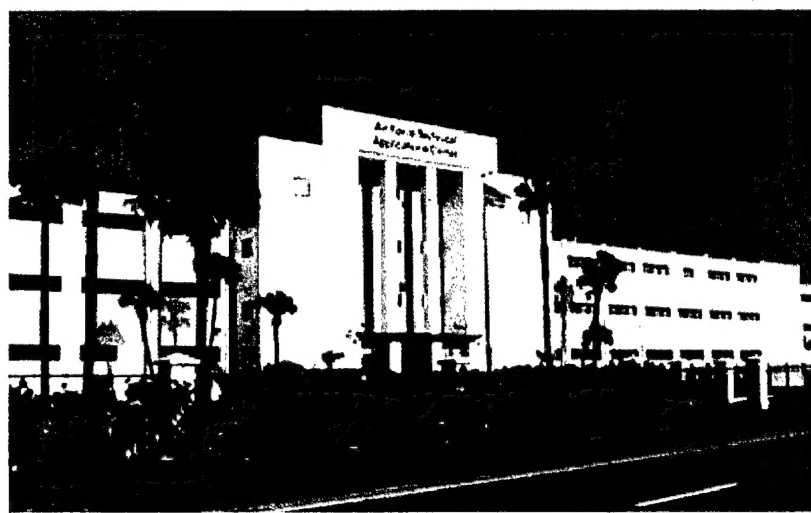
A Plan of Development for Detection Systems for Seismic and Infrasound Arrays

Robert R. Blandford

8 April 2002

20031217 224

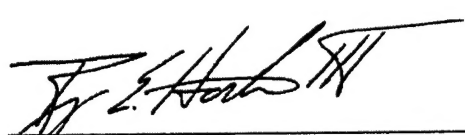
Approved for Public Release;
Distribution is Unlimited



Report AFTAC-TR-02-007 has been reviewed and is approved for publication.



DAVID R. RUSSELL, SES
Director, Nuclear Treaty Monitoring



ROY E. HORTON III, Colonel, USAF
Commander

The overall classification of this report is UNCLASSIFIED

Addressees: Please notify AFTAC/TT, 1030 S. Highway A1A, Patrick Air Force Base FL 32925-3002, if there is a change in your mailing address (including an individual no longer employed by your organization) or if your organization no longer wishes to be included in the distribution of future reports of this nature.

REPORT DOCUMENTATION PAGE

*Form Approved
OMB No. 0704-0188*

Public reporting burden for this collection of information is estimated to average 1 hour per response, including the time for reviewing instructions, searching existing data sources, gathering and maintaining the data needed, and completing and reviewing this collection of information. Send comments regarding this burden estimate or any other aspect of this collection of information, including suggestions for reducing this burden to Department of Defense, Washington Headquarters Services, Directorate for Information Operations and Reports (0704-0188), 1215 Jefferson Davis Highway, Suite 1204, Arlington, VA 22202-4302. Respondents should be aware that notwithstanding any other provision of law, no person shall be subject to any penalty for failing to comply with a collection of information if it does not display a currently valid OMB control number. PLEASE DO NOT RETURN YOUR FORM TO THE ABOVE ADDRESS.

1. REPORT DATE (DD-MM-YYYY) 8 April 2002				2. REPORT TYPE Technical		3. DATES COVERED (From - To)	
4. TITLE AND SUBTITLE A Plan of Development for Detection Systems for Seismic and Infrasound Arrays				5a. CONTRACT NUMBER			
				5b. GRANT NUMBER			
				5c. PROGRAM ELEMENT NUMBER			
6. AUTHORS Robert R. Blandford				5d. PROJECT NUMBER			
				5e. TASK NUMBER			
				5f. WORK UNIT NUMBER			
7. PERFORMING ORGANIZATION NAME(S) AND ADDRESS(ES)				8. PERFORMING ORGANIZATION REPORT NUMBER AFTAC-TR-02-007			
Air Force Technical Applications Center (AFTAC/TT) 1030 S. Highway A1A Patrick AFB FL 32925-3002							
9. SPONSORING/MONITORING AGENCY				10. SPONSOR/MONITOR'S ACRONYM(S)			
				11. SPONSOR/MONITOR'S REPORT NUMBERS			
12. DISTRIBUTION/AVAILABILITY STATEMENT Approved for Public release; Distribution Unlimited.							
13. SUPPLEMENTARY NOTES							
14. ABSTRACT A review is given of standard array design and signal processing for teleseismic and regional seismic arrays. The review is extended to F and correlation detection for seismic and infrasound arrays, to array design for infrasound arrays, and to optimal detection on single channels. With this background, a plan of development is suggested which will bring seismic and infrasound array detection processing fully up-to-date with the procedures recommended by the latest research. Suggestions are also made as to the proper design of new infrasound arrays.							
15. SUBJECT TERMS Infrasound Arrays Seismic Detection Systems							
16. SECURITY CLASSIFICATION OF:			17. LIMITATION OF ABSTRACT	18. NUMBER OF PAGES	19a. NAME OF RESPONSIBLE PERSON Robert R. Blandford		
a. REPORT	b. ABSTRACT	c. THIS PAGE			19b. TELEPHONE NUMBER (include area code) (703) 648-6789		
Unclassified	Unclassified	Unclassified	Unclassified	64			

(This page intentionally left blank.)

CONTENTS

	<u>Page</u>
List of Figures	vii
Acknowledgments	viii
Introduction	1
Standard Array Design and Processing for Seismic Detection	2
Array Design	2
Teleseismic Array Design	2
Regional Array Design	4
Beam Type	5
Coherent Beams	6
Incoherent Beams	6
Filtering	7
Detection Trigger	7
Azimuth Estimation	8
Detection and Feature Extraction (DFX)	8
<i>F</i> Detection for Seismic Arrays	9
Theory of Qualitative Behavior of <i>F</i> Detector	9
Special Cases	9
False Alarm Rates and Probability of Detection for <i>F</i>	11
Application of <i>F</i> Detector at the Tonto Forest Seismic Observatory	11
Effects of Side Lobes on Power and <i>F</i> Detectors	12
Infrasound Arrays and Detection	13
Historical Arrays and Processing	13
Beamforming, Relation of <i>F</i> to Average Correlation	13
Modifications of DFX to Compute <i>F</i>	14
Observed Infrasound Noise and Signal Correlation and S/N	15
Aperture and Sidelobes	16
Detection on Single Channels	17
Suggestions for Development	19
Seismic Detection System Development	19
Infrasound Detection System Development	20

CONTENTS (Continued)

	<u>Page</u>
Figures	21
References	39
Distribution	43
Appendix: Correlation of 23 July 1999 Shuttle Event at DLIAR	A-1

LIST OF FIGURES

	<u>Page</u>	
Figure 1	Configuration of the early Geneva-type observatories	22
Figure 2	Configuration of early LASA design	23
Figure 3	Signal and noise correlation estimates from a temporary array deployed near the NORESS site	24
Figure 4	The geometry of the NORESS array	25
Figure 5	Gain curve (from Kvaerna, 1989)representing the best gain values produced by any of 10 NORESS subgeometries tried	26
Figure 6	NORESS Beam Deployment Table	27
Figure 7	TFSO 37-element array in Arizona	28
Figure 8	3 dB contour of the short-period TFSO Kurile beam	29
Figure 9	Detector response traces	30
Figure 10	Power-slowness and F plots of a Fox event	31
Figure 11	Power-slowness and F plots of the Fox event	32
Figure 12	Raw and filtered traces of two shuttle launches	33
Figure 13	Signal and noise spectra of the DLIAR 23 July 1999 shuttle signal	34
Figure 14	Signal and noise spectra for the Lac du Bonnet 27 May 1999 shuttle signal	35
Figure 15	Wavenumber 1 Hz power spectrum of the DLIAR array	36
Figure 16	Wavenumber 1 Hz power spectrum of the augmented DLIAR array	37
Figure 17	Wavenumber 0.5 Hz power spectrum of the augmented DLIAR array	38
Figure A-1	Shuttle Signal at DLIAR, 23 July 1999, 0.2Hz HP	A-4
Figure A-2	Shuttle Signal at DLIAR, 23 July 1999, 0.8-1.2 BP	A-5
Figure A-3	Shuttle Signal at DLI04, 23 July 1999	A-6

ACKNOWLEDGMENTS

Thanks to Al Bedard for information on the N4 correlator; to Richard Stead, Greg Wagner, and Darrin Wahl for guidance through the complexities of DFX; to David McCormack for Lac du Bonnet shuttle data and for computation of correlations for that data; and to Jin Wang for his mat-lab array response routine.

INTRODUCTION

The theory and practice of seismic array design, and of event detection at seismic arrays, are subjects with a long history. Studies began well before the installation of the Large Aperture Seismic Array (LASA) in Montana in 1965 and, with one or two recent exceptions, seismic array design theory was brought to a mature state by workers in Norway and the US in the 1980's. In particular, array design methods developed in this time interval were elegantly used to design NORESS.

In the course of building operational arrays and selecting processing methods, some detection processing methods which promised a few decibel (dB) improvement in detection thresholds were not implemented. The reason for this was that there were many practical obstacles to good performance, such as dealing with data glitches and local events, detecting later phases, and identifying those phases which were detected. It was thought prudent to solve those practical problems before attempting to implement refinements.

At this point in time (the year 2000), there are two reasons to revisit the subject of threshold improvement: (1) substantial effort has gone into solution of the practical obstacles outlined above; (2) software processing systems have been constructed which are robust enough that additional processing can be coded and tested in an operational environment fairly easily; and (3) a worldwide network of infrasound arrays are to be installed *de novo*. It is important that existing and new methods of array design be exploited properly so that these infrasound arrays will be installed with proper designs the first time. We also should begin to exploit processing methods which promise improved thresholds but which have not, to date, been fully tested.

The outline of this report is that first we review the current standard of seismic array design, and the operational detection techniques, both coherent, incoherent, and single-channel, which are in place today.

We then discuss the properties of the "F Detector" process and possible benefits which might result from applying it for seismic and infrasound arrays. Following this, we discuss the different, not currently implemented, methods of detecting on individual traces, including optimal frequency filtering and stabilization of the false alarm rate.

Finally, we recommend combinations of array and single channel processing techniques which should be tested for implementation, and also discuss how existing array design techniques should be applied for the planned international network of infrasound arrays and for special seismic applications.

STANDARD ARRAY DESIGN AND PROCESSING FOR SEISMIC DETECTION

Array Design.

Among the first seismic arrays were those built to specifications recommended by the Geneva Conference of Experts in 1958, see, e.g., Carpenter (1965). The dominant noise on short-period surface vertical instruments in most systems existing then was caused by wind, and it was known from studies (C. Romney, personal communication; Blandford and Clark (1971)) that wind-generated noise was uncorrelated at a spacing of approximately 0.6 kilometers (km). (This analysis was actually originally performed by observing Lissajou figures on an oscilloscope!)

Due to lack of computer power, it was desired to cancel the noise by direct summation of the analog traces so as to form an infinite velocity teleseismic beam. Therefore, the instruments had to be spaced closely enough that the signals were substantially in phase. A velocity of 12 km/second (sec) with moveout less than one-quarter cycle at 1 Hertz (Hz) would imply an array 3 km in diameter. Thus, the Geneva arrays (e.g., Blue Mountain Seismic Observatory (BMSO)), shown in Figure 1, have a diameter of 3 km or less, and a minimum spacing on the order of 0.5 km. The minimum spacing was actually selected to be somewhat greater than 0.5 km because, when there was little wind, the propagating mantle P wave seismic noise, which remains correlated to greater distances, becomes an appreciable fraction of the total noise background.

Subsequent array designs have been more sophisticated, but have not exhibited superior physical insight or better matches to the available computer power.

Teleseismic Array Design.

The next array design (Green *et al.*, 1965; Frosh and Green, 1966), the design for the LASA in Montana, was performed under conditions of a perhaps inadequate understanding of the signal and noise character. As a result, the array as built did not meet expectations.

Figure 2 shows the design of the array as built. The subarray design was constrained by the desire to reject coherent surface Raleigh waves with velocities between 2.5 and 4.0 km/sec, and frequencies between 0.2 and 5.0 Hz. To avoid spatial aliasing, a minimum spacing of 0.5 km was required. To make the subarray beam narrow enough that a teleseismic beam could reject Raleigh waves at 0.2 Hz, it was necessary to have a diameter of 7 km. Assuming a geometrical layout of six radial arms of seismometers, approximately 25 instruments per subarray were needed.

As slightly more than 500 seismometers were readily available, it was possible to have 21 subarrays. The maximum array diameter of 200 km was selected in order to give a reasonable teleseismic location capability assuming perfect signal correlation. The subarrays were placed on a logarithmic spiral so that the beam width would be approximately constant with signal wavelength. The constant for the spiral was chosen so that there would be an approximately uniform density of subarrays and elements at the center of the array.

Green (1965) recognized that if the signal correlation was low, a reduced diameter array would still contain a large number of seismometers.

What were the flaws in this array design? First, the array was designed in order to reject coherent microseismic noise, with peak frequency near 0.2 Hz, while passing a teleseismic signal undistorted. This noise is very high in amplitude and, therefore, its spectral matrix must be very stable in time; the instruments, local site installation, and site geologies must be very well matched; and the processing must be very high in precision, in order that a multichannel processor based on a preceding noise estimate can reduce subsequent noise at 0.2 Hz to an amplitude comparable to the noise displacement amplitude at 1 Hz. Otherwise, while there may be improvements in discrimination for larger signal-to-noise (S/N) events based on a more complete picture of the waveform as a function of frequency, there would be only minimal improvement of detection over that obtained by a bandpass filter centered at 1 Hz. This is because improvement of the detection threshold requires detection of smaller events, with approximately flat displacement spectral shapes, at the margin of detection. Despite considerable effort by workers at Texas Instruments and Lincoln Labs (see, e.g., Capon *et al.* (1968)), this large reduction in 0.2 - 0.8 Hz noise could not be accomplished. Therefore, nearly equivalent S/N and bandwidth could be achieved simply by high-pass filtering.

Once it became clear that the closely-spaced LASA subarray seismometers were not needed to reject 0.2 Hz Raleigh waves for detection, it also became clear that the seismometers were too closely spaced for simple beamforming for $N^{1/2}$ noise reduction at 1 Hz; the correlated noise between the closely spaced sensors reduced the beam S/N. As a result, the inner two rings, 9 of the 25 sensors in each subarray, were removed soon after installation. Even more sensors and outer subarrays were removed in subsequent years of operation as it became clear that the closely-spaced sensors introduced correlated noise, and the outer subarrays contributed little due to poor signal correlation. See, for example, Blandford and Clark (1971, 1975).

A second flaw in understanding of the signal and noise was, as Green (1965) may have suspected, that signal correlation across the 200 km aperture was poor at 1-2 Hz, where the peak S/N is located for teleseismic events. See, for example, Capon *et al.* (1968), who point out a 9-to-1 variation in signal amplitude across the full array; and Flatte and Wu (1988), who conclude that at NORSAR at 2 Hz the root-means-square (rms) log amplitude fluctuation is 0.41 with a coherence scale less than 18 km. Flatte and Wu also find that the coherence scale for phase (arrival time variation) is equal to 18 km. Since 18 km is much smaller than the 200 km aperture of LASA, it is very likely that a smaller array would give more precise slowness estimates for an equal number of deployed seismometers. The increased signal coherence would result in a greater gain in azimuth estimation precision than the decreased aperture would lose. A theory which makes possible a quantitative assessment of this idea has recently been developed by Shumway *et al.* (1999).

Regional Array Design.

The NORESS array was the first array designed with monitoring of high-frequency regional seismic signals in mind. Among the first to survey the correlation of signal and noise with a view toward regional array design were Mrazek *et al.* (1980) and Der *et al.* (1984). However, the first actual design of a regional array began with a survey of signal and noise correlation by Mykkeltveit *et al.* (1983), as exemplified in Figure 3. We see that the maximum distance for a fixed value of signal or noise correlation is a function of frequency.

With these data in hand, Mykkeltveit *et al.* were able to calculate G^2 , the power gain in S/N, as

$$G^2 = \frac{1 + (N - 1)\bar{c}}{1 + (N - 1)\bar{\rho}}$$

where N is the number of elements in the array, and \bar{c} and $\bar{\rho}$ are the average correlation over all array element pairs of the signal and noise correlation, respectively.

The overall design procedure is described in Mykkeltveit (1985) where he estimates the parameters for the array from a family of array geometrical designs suggested by Followill and Harris (1983).

Quoting from Mykkeltveit (1985):

"They proposed a geometry based on concentric rings spaced at log-periodic intervals in radius R , according to the relation:

$$R = R_{min} \cdot \alpha^n \quad n = 0, 1, 2, 3.$$

"Their design includes the deployment of an odd number of elements symmetrically distributed in azimuth, and it has the following attractive features:

"With an odd number of elements in each ring, the corresponding co-array (defined as the set of all intersensor separations in vector space) pattern has no overlap among its points, *i.e.*, it samples the wavefield in the best possible way, in this respect.

"Designs based on (the above formula) comprise comprehensive subsets of sensors with very different typical intersensor separations, implying that both high-frequency and low-frequency phases could be well-enhanced by appropriate subsets of the array.

"The beam patterns for the above designs are favorable, with narrow main lobe yielding good resolution in phase velocity and azimuth and absence of cumbersome side lobes."

The constants in the above equation were evaluated in order to maximize the S/N for selected frequencies and phases. In addition, the loss of correlation of the signal was reported to have been used to evaluate the width of detection beams as a function of array aperture. This was used as a proxy for the loss of location capability as a function of array aperture, and results in an optimum intermediate aperture; location capability does not increase indefinitely as array aperture increases. A similar analysis was reported on in detail by Mrazek *et al.* (1980).

These analyses yielded the optimum design seen in Figure 4, for which $R_{min} = 0.15$ km and $\alpha = 2.15$.

There are a couple of minor criticisms possible with respect to this design.

First, the signal correlations seen in Figure 3 are, in part, suspect. We see that the Pn correlation is worse at 0.8-2.8 Hz than it is for 2.4-4.8 Hz. This almost certainly reflects poor S/N at the lower frequencies and is not a characteristic of the signal itself. As support for this interpretation, Kvaerna (1989) and Harjes (1990) show much higher correlation, and the correlation decreases as frequency increases.

A second critique is that the half-width of the beam is not actually a good measure of an array's location capability. A better approach, in effect, looks at the roughness due to noise and lack of signal correlation near the peak of the lobe. This roughness limits the precision to which the peak may be found. The analysis may be found in Shumway *et al.* (1999), and is applied to infrasound array design by Blandford (1997, 2000).

Harjes (1990) showed correlations for Pn, Pg, and Lg in the passbands 1-2 Hz and 2-4 Hz for distances out to 3 km. Roughly speaking, correlations remained above 0.9 for Pn and Pg all the way to 3 km. For Lg, the correlation was >0.9 for 1-2 Hz, and roughly >0.8 for 2-4 Hz.

These correlation values, considered together with the noise correlations seen in Figure 3, would support a minimum spacing of 1 km (instead of the 0.15 km found in the NORESS design) in that noise would be cancelled for low (*e.g.*, teleseismic) frequencies, but little significant signal would be lost up to 4 Hz.

This was one of the considerations in the design of the new International Monitoring System (IMS) seismic stations, some of which have two rings of three and five elements each, for a total of nine elements; the radius of the innermost ring is 1/3 to 1/2 km and the radius of the outermost ring is 2 km.

It may be noted that such an IMS array design seems to be on the verge of undersampling in space for some signals of interest, for example, a 3 Hz Lg may have a wavelength of 1 km. However, array responses show that, even in this case, all side lobes in the velocity and frequency ranges of interest are down about 6 dB or more which, as we shall see, should prove sufficient to decide on which beam a strong detection arrived or, for a weak signal, to cause no detection to occur on a side lobe.

Beam Type.

Given an array design, the next step is to determine a suitable beam deployment. For NORESS, the results of such an analysis is presented by Mykkeltveit *et al.* (1990).

An indication of the approach taken by Mykkeltveit *et al.* to determine the beam deployment was given by Kvaerna (1989) who determined the elements of NORESS which should be included at each frequency band in order to detect teleseismic and regional P waves.

Coherent Beams.

Figure 5, from Kvaerna (1989), shows the empirically determined NORESS elements which result in the highest S/N as a function of frequency. The S/N represents the best combination of signal loss (SLOSS) and noise suppression (NSUPP). We see that for high-frequency (5-10 Hz regional) P waves there is roughly 4 dB of signal loss in the optimum array, which comprises all 25 elements of this 3 km aperture array. It is noteworthy that, at these frequencies, the A ring, at 150 meters radius, appears to contribute fully to the expected $N^{1/2}$ noise suppression of 14 dB.

Figure 6 shows the table of NORESS Beam deployments from Mykkeltveit *et al.* (1990). Quoting from Mykkeltveit *et al.*:

"The NORESS beam deployment in use since 13 April 1989 is given in (Figure 6). It is composed of 76 beams, of which 66 are conventional, coherent ones. These 66 beams are aimed at detection of P phases at all frequencies, and are designed and deployed in accordance with the criterion that the gain loss due to missteering should be less than 3 dB for any signal from any direction, arriving at NORESS with an apparent velocity above 6.0 km/sec. The subconfiguration defined for each of these beams is the one that has been found to provide the best SNR [signal-to-noise ratio] gain for the frequency band in question (see Kvaerna, 1989).

"It is found ... that the Pn and Pg phases are best observed on vertical channels but in different frequency bands (here: 10 to 16 Hz for Pn and 3.5 to 5.5 Hz for Pg). The Lg phase stands out clearly in the 1 to 2 Hz band, also on vertical channels"

Incoherent Beams.

Continuing the discussion of Mykkeltveit *et al.* (1990):

"The onset of the Sn phase, however, is very often found to have an impulsive character on the horizontal channels and in a relatively high filter band (here: 5 to 8 Hz) ... Incoherent beams are particularly suited for detection of secondary phases, which are often of an emergent nature. Ten such beams are included in the NORESS beam set, and are specifically aimed at detecting Sn (beams NH01-04) and Lg (beams NV01-06) arrivals. Details on incoherent beamforming are given in Ringdal *et al.* (1972, 1975)."

Ringdal *et al.* (1975) conclude that "incoherent beamforming at NORSAR is generally superior to conventional beamforming in detecting near-regional seismic events ... and very high frequency signals."

Despite the above empirical conclusion, theory developed in Ringdal *et al.* concluded that incoherent detectors would be substantially inferior to a detector on a well-correlated signal. However, Wirth *et al.* (1971, 1976) concluded theoretically that an incoherent detector could be nearly equal in capability to that of a coherent detector on a perfectly correlated signal. Their theoretical conclusion is therefore in agreement with the empirical conclusions of Ringdal *et al.*

The differing thresholds seen in Figure 6 are determined, as discussed by Kvaerna *et al.* (1987), by running the differing beams on a noise sample believed to contain no signals. The thresholds are adjusted so that there is an equal false alarm rate on each beam.

Filtering.

Vanderkulk *et al.* (1965), drawing on the work by Freiberger (1963), assumed that the optimum frequency pre-filter for detection of weak signals is of the form $S(f)/N^2(f)$, where S and N are the signal and noise amplitude spectra. N can be estimated directly as the noise in the absence of signal, and S can be estimated by the product of the source spectrum (flat to displacement for small events) times the instrument response, times attenuation.

Because the attenuation is less for regional signals, the optimum filters for regional signals pass more high-frequencies.

There may be special situations where the above recipe for estimating S is not correct; for example, for some phases, *e.g.*, Lg or LR, the source function is shaped by the response of the earth. Or, as another example, the site response may have a resonance. In those cases, it may be necessary to observe S directly for a large event and to use some means to extrapolate the signal shape to that which would be appropriate for smaller sources.

Vanderkulk *et al.* (1965) concluded that a suitably selected bandpass filter could be sufficiently close to the optimum filter that only about 1 dB would be lost in threshold. A similar result was obtained by Mykkeltveit and Bungum (1984). As a result, with only one exception of which I am aware (*i.e.*, the AFTAC TOSS system), bandpass filters have been used as filters in most operational systems.

It seems worth remarking at this point, however, that an updated optimal filter could take advantage of changes in noise spectral shape, *e.g.*, from changes in the wind or cultural noise sources. This could be a substantial practical advantage over and above any small advantage the optimum filter might have when N is unchanged in time.

Detection Trigger.

The standard approach to detection on a beam was perhaps first implemented by workers at IBM: IBM (1972), Vanderkulk *et al.* (1965). In that approach, the beam was rectified and an average (STA) over a short time period, *e.g.*, 1 second, was computed.

Then the STA was recursively smoothed with a time constant of perhaps 30 seconds to form the long-term-average (LTA). Detection was performed for excursions over a threshold of the STA/LTA.

Vanderkulk showed that rectifying instead of squaring the beam (which is the optimum process according to detection theory) only degraded the detection threshold by less than 1 dB. Since rectification was less costly in computer processing, and was also less vulnerable to noise spikes, rectification was adopted as the standard.

Azimuth Estimation.

In the LASA system, the detection azimuth was determined as the beam on which the highest STA was observed. However, with the advent of incoherent processors, STA values for different beams became incommensurable. Therefore, a new method of azimuth estimation was developed in which a broadband fk spectrum was calculated after each detection, and the maximum amplitude peak was selected as the azimuth. This approach is discussed by Kvaerna and Doornbos (1986). Of course this method may give poor results for poor S/N events detected on incoherent beams.

Detection and Feature Extraction (DFX).

The DFX system (Wahl, 1996a,b) embodies many of the detection ideas that we have discussed in this section. One may specify beams, as in Figure 6; specify the STA and LTA integration times; rectification or squaring of the beam; and specify that a beam be coherent or incoherent.

DFX also offers the option of detecting using the "Z" or "log Z" statistic instead of using STA/LTA (Blandford, 1981; Shensa, 1977). For the "Z" statistic, the standard error of (STA-LTA) is recursively estimated and divided into the difference (STA-LTA). For the "log Z" detector, the STA is replaced by $\log(\text{STA})$, the LTA is a recursive estimate of $\log(\text{STA})$, and the standard error is estimated on the difference. A working hypothesis is that the resulting variables have a normal distribution, and this provides some guidance in setting thresholds. Lacoss (1972) may be credited with originally developing the concept of holding the false alarm rate constant by normalizing detecting on a variable normalized by its estimated variance.

Also, the fact that the standard error is recursively updated can, in principle, provide some ability to hold the false alarm rate constant under changing noise conditions which may increase or decrease the bandwidth of the noise and, thus, the variability of the STA, as seen through the detection filter.

The background and relative performance of these different detection statistic approaches are discussed in the "Detection on Single Channels" section later in the report.

F DETECTION FOR SEISMIC ARRAYS

Despite the historical dominance of the simple STA/LTA detection procedure outlined in the preceding section, there has been a modest amount of research into the "F" detector, see Blandford (1974) for history.

Instead of estimating the LTA from past noise, the F detector estimates the noise from data in the same time interval which defines the STA.

It performs this neat trick by subtracting the beam, suitably time-shifted, from each individual channel. If there is perfect correlation, and if the moveouts are perfectly estimated, then the residual is the noise "under" the signal. This noise is averaged over all channels and this then forms the noise estimate or "LTA" although it is not, of course, averaged over a long time.

The F detector does not, in theory, have a higher probability of detection for a fixed false alarm rate than does the STA/LTA detector. However, it has a number of appealing qualitative properties which may be of practical importance and which may, in fact, lead to lower thresholds

Theory of Qualitative Behavior of F Detector.

To begin to discuss the qualitative properties of the *F* detector, let B represent the power of the filtered beam averaged over some time window. Let P represent the average of the M filtered single-channel powers, averaged over the channels. Then,

$$F = (M - 1) \frac{B}{P - B}$$

This formula is valid if the expected value of the trace means is zero. This will be the case for the filtered traces which are of interest for our application.

The denominator has, as displayed above, been algebraically simplified from a different expression which may be more easily understood from a physical point of view. That expression is the difference between an individual channel and the beam waveforms, squared and averaged over time and over channels.

It is clear from this latter formulation that the denominator amounts to the residual noise. It is also clear that, unless the channels are well correlated, the denominator will be larger than the noise and that F will not reach the maximum possible value.

Special Cases.

We will now discuss several cases of interest:

First, what is the value of F when there is an identical signal with power S^2 on the N channels, and no noise? This corresponds to the arrival of a high S/N event. In that case, $B = P = S^2$ and F is infinite.

Next, what is the value of F when all channels are zero except for one channel with power S^2 ?

This corresponds to a large spike on a single channel. In that case, $P = S^2/M$; $B = S^2/M^2$ since the signal amplitude is S and the beam amplitude is therefore S/M . Then, doing the simple algebra, we find that F is identically 1. So a large spike does not cause the F statistic to fluctuate above 1.0 which is, as we shall see next, the expected value of F in the presence of uncorrelated noise. Thus, data glitches (and large off-beam events) will not cause an F detector to generate a spurious detection.

Next we estimate the value of $E(F)$, the expected value of F , when there is random uncorrelated noise on each channel with expected amplitude 1.

We know that $E(B) = 1/M^2$, and $E(P) = 1$. Again, doing the simple algebra, we find that $E(F) = 1$. So, in the absence of signal, and in the presence of uncorrelated noise, the expected value of F is 1.0.

A useful point is that this result also shows that if F is input as the STA to an STA/LTA procedure, the threshold on STA/LTA is expected to be identical to the threshold for F alone since $LTA=E(F)=1$.

Before going on to determine thresholds from the statistics of the F distribution, let us consider a final case: a poorly aligned strong signal. Consider the case of only two channels, $M=2$. Let the signal be of the form [1 -1]. For this signal, $P=2$. We know that if the channels are perfectly aligned, then B also is 2 and F is infinite. But consider the case when the channels are aligned one step off so that the 1 from the first channel is aligned with the -1 from the second channel. Then the beam is [1/2 0 -1/2]. Then, averaging over a window which covers the signal plus some time to spare, B is 1/2, and $F = (1/2)/(2-1/2) = 1/3$.

Thus, in the presence of an off-beam signal, F can be less than 1.0. This illustrates the F response well away from the main lobe or a side lobe.

This result is reminiscent of, but not the same as, a result from Smart and Flinn (1971) giving a limit on the value of F on a side lobe with relative power, f .

$$F < (M-1) * [f/(1-f)]$$

For example, for a 9-element array, if all side lobes are down 6 dB, a factor of 2 in power, then $F < 8/3 = 2.66$. Since typical short-period seismic F thresholds for false alarm rates of a few per day are in the neighborhood of 10, there is no risk of triggering a detection on a main beam from a signal which arrives on a side lobe.

In addition, if, after F detection, azimuth estimation consists of running an fk spectrum in which F is computed, and if all side lobes are down 6 dB, there will be one peak, the correct peak, for which both power and F are larger than the side lobes.

False Alarm Rates and Probability of Detection for F.

F is distributed as the ratio of two χ^2 statistics and, in the absence of signal, may be notated as $F(D_1, D_2, 0)$. $D_1 = 2WT$, where W is the filter bandwidth and T is the time over which B and P are averaged, are the degrees of freedom for the numerator (B), and $D_2 = (M-1)*2WT$ are the degrees of freedom for the denominator, (P-B). See, for example, Shumway (1971, 1988).

The zero (0) in $F(D_1, D_2, 0)$ expresses the fact that in the absence of signal, the F distribution has non-centrality parameter, $\lambda = 0$. In the presence of signal with signal-to-noise amplitude ratio S/N, $\lambda = 2WT(S/N)^2$.

A specified false alarm rate, FAR, may be set by solving for the threshold, T, such that:

$$P\{F(D_1, D_2, 0) \geq T\} = FAR$$

Then the probability of detection, PD, is given by

$$P\left\{F(D_1, D_2, 2WT(S/N)^2) \geq T\right\} = PD$$

Application of F Detector at the Tonto Forest Seismic Observatory.

An illustration of the F detector in operation at the Tonto Forest Seismic Observatory (TFSO) in Arizona was reported by Blandford (1974).

Figure 7 is a plot of the deployed short period vertical instruments. The data were filtered 0.5 to 1.5 Hz; the dominant frequency seen through the filter was 1 Hz. Figure 8 is a plot of the 3 dB contour for the beam on which the F detector operated.

Figure 9 illustrates some of the qualitative properties of the F detector as discussed in the previous section. The upper set of four traces shows a clear signal arriving on trace #3, which is the beam directed at the Kuriles. The signal is weak enough that little trace of it can be seen on traces #1 and #2 which are beams directed to other source regions.

Trace #4 is the value of the F statistic, and we see that it rises to a level substantially greater than the preceding noise fluctuations, suggesting detection.

The bottom four traces illustrate the F detector's response, #4, on the Kurile beam, #3, to a large signal arriving on a Hindu-Kush beam, #2. We see the maximum amplitude on beam #2, and a substantial leakage signal on #3.

Despite the substantial leakage on #3, the F statistic on #4 does not rise and, in fact, appears to be depressed below the noise level. This is in agreement with the qualitative behavior discussed in the preceding section.

Analysis of a month's output from this F detector revealed that the detector had a false alarm rate in accordance with theory for the selected threshold, approximately 0.2 false alarms per day, and a detection capability comparable to that of a human analyst. In addition, there were no false detections due to data glitches or to side lobe detections.

The excellent detection performance of the F statistic at TFSO implies that the noise correlation is close to 0.0, and the signal correlation at 1 Hz, over the 30 km aperture of TFSO, is close to 1.0. While good signal correlation at these distances seems somewhat surprising, I have not been able to find good evidence to the contrary in the literature; most published results are for bandpasses at higher frequencies.

In any event, this example suggests that, in some cases at least, the good qualitative properties of the F detector may be merged with quantitatively good detection capability. Each application will have to be judged on its own merits.

It is clear that the F detector will be unsuitable for detecting some array-frequency-phase combinations, *e.g.*, those for which Mykkeltveit *et al.* (1990) determined incoherent beams to be optimal at NORESS. If an incoherent beam is superior to a coherent beam, then correlation is presumably low and an F detector is unlikely to work well. On the other hand, for those beams for which Mykkeltveit *et al.* found coherent beams to be optimal, the F detector is likely to work.

Effects of Side Lobes on Power and F Detectors.

To investigate the effect of side lobes on use of the F detector, Blandford (1972) investigated the fk and F plots for selections of sensors from TFSO. Using a 1 Hz Fox Islands teleseismic event with a wavelength of approximately 14 km, Figure 10 illustrates the response of a 7-element array comprising the center element and every other sensor in the second ring of TFSO (see Figure 7). This array will have minimum spacings only slightly smaller than the wavelength, so some aliasing is expected.

In Figure 10a, the main lobe is in the Northwest direction, but we see three other side lobes, two of them less than 1 dB down.

In Figure 10b, we see the F spectra; we see that there are large values of F at each of the side lobes, so that it would be difficult to determine the true direction of approach of the signal.

A standard approach to reducing side lobes is to introduce a few sensors at closer spacings in order to improve sampling. In this case, we add sensors 4, 5, and 6 which, together with sensor 1, form a 5 km on a side parallelogram array.

Figures 11a,b show that this addition reduces the power side lobes to a degree sufficient to also reduce the F statistic below levels which would be above a detection threshold.

INFRASOUND ARRAYS AND DETECTION

Historical Arrays and Processing.

From approximately the 1950s up until the 1970s, the Air Force Technical Applications Center, together with other agencies of the US Government, operated a worldwide network of infrasound arrays. Generally, these arrays consisted of four elements in a rectangle 10 km on a side. Data were produced in two passbands, flat to pressure: one from 100 seconds to 10 seconds, and a second from 30 seconds to 1 second.

Initially, the records were played out on stripcharts and analyzed visually. If the stripcharts were transparent, the traces could be overlaid in order to correlate waveforms and determine the relative signal delays. With a set of delays, the back azimuth could be obtained.

In the later stages of the network, an N4 correlator, Melton and Bailey (1957), Brown (1963), Bedard and Caldwell (1970), was used to analyze the data. Input to the correlator was from magnetic tape. Moveable heads were used to introduce delays, and the output from these heads could be frequency-filtered and summed for a range of slownesses and azimuths. This process amounted to continuously computing a set of frequency-filtered beams. Presumably a peak in the beam would lead to manual inspection of the individual traces to detect correlation.

Since the signals of greatest interest were typically in the period range of 100-30 seconds, with wavelengths of perhaps 30-10 km, the signals were generally adequately sampled in space and there was no spatial aliasing problem.

Correlation must be used as a detector in addition to power (as is done for seismic systems) because most infrasound noise is due to pressure fluctuations advected by the wind and, as a result, there are frequent large bursts of noise on the sensors. A power detector will trigger on these bursts, and this would introduce a high false alarm rate. Noise bursts do not introduce increases in correlation.

Beamforming, Relation of F to Average Correlation.

As we have seen in the discussion of the qualitative properties of F, high values of F are associated with high values of correlation. In fact, Katz *et al.* (1999) has shown that the expected values of F and $(M-1)(c/(1-c))$ are equal, where c is the average cross-correlation.

We see that there are two different ways to compute an F detector: either as an average over correlation pairs for a set of beams, or as implicit in the formula $F=(M-1)(B/P-B)$ discussed previously.

The resistance of the F detector to noise bursts corresponds to the resistance of correlation to noise bursts.

Modifications of DFX to Compute F.

In the DFX system (Wahl, 1996a,b), beamforming and filtering take place in the C routine beam_create which resides in the file beam.c in the library libbeam.

The routine beam_create returns a filtered beam which is, for short-period seismic data, typically 15 minutes long, to the C routine compute_stav which resides in the file stav.c in the library libdetect. The routine compute_stav actually computes a time series of STA values from the returned beam.

In order to compute F instead of STA in compute_stav, it is necessary to return to compute_stav the 15-minute time series of the average single station power, P, in addition to the beam.

As it happens, this is easy to arrange, since the beam is calculated within beam_create by sequentially adding time-shifted and filtered channels into the time-indexed beam vector until all channels have been added. Immediately after a channel has been added to the beam, it may then also be squared and added to a new time-indexed vector which becomes P after all channels have been added. This additional computation to compute P is almost negligible when compared to other processing, *e.g.*, filtering, which occurs in beam_create. Then P may be passed back to compute_stav along with the beam.

It has often been thought that it could be expensive in computer time to compute F if there were a large number of beams as compared to channels because, instead of having only to filter the beam, it is necessary to filter the individual channels.

Since this filtering of individual channels must also occur for incoherent beams, incoherent beams in the existing DFX system require extra computation as compared to coherent beams.

All the filtering in DFX occurs within beam_create, and the existing DFX structure makes it unclear how difficult it would be to alter the system in order to filter the channels, before a series of calls to beam_create, as a preparation for computing a large number of beams for one filter and one time period.

We may modify DFX to remove this extra computational cost by statistically storing the filtered channels within beam_create, and by checking the input parameters each time beam_create is entered to see if the existing filtered data can be reused. Since several beams, *e.g.*, for a range of azimuths and slownesses, for a fixed filter are typically called sequentially, it is usually the case that the filtered channels can be reused.

As a result of these modifications to DFX, calculation of F and of incoherent beams will not generally require significantly more computation than do standard beams.

Observed Infrasound Noise and Signal Correlation and S/N.

Mack and Flinn (1971), using data observed at the Large Aperture Microbarograph Array (LAMA), collocated with LASA, assumed that an arriving signal could be represented as a distribution in wavenumber space.

Assuming that the signal had a spread in azimuth of 5° , and a spread in slowness of 0.015 km/sec, this approach yielded theoretical curves which matched coherence measurements for intersensor spacings of 50 to 7 km, and periods of 100 to 10 seconds.

Blandford (2000) reported that historical data recorded at a 1 km aperture array 700 km from a 2.6 kiloton (kt) nuclear explosion in the South Pacific confirmed the Mack-Flinn coherence expressions, and showed good S/N at 2 and 1 seconds period.

However, the historical data was of marginal quality at 1 Hz, and the distance range was too short to comfortably be applied to the IMS network of stations which typically are separated by 2000 km.

This latter point is especially critical, since many signals observed from distances near 500 km exhibit excellent correlation at 2 and 3 km spacing for 1 Hz, whereas the Mack-Flinn relation predicts poor correlation. See, for example, Blandford (2000). The tentative explanation for this paradoxical result is that the closer signals are not scattered into as large a region of wavenumber space as are the more distant signals. Nonetheless, any convincing data must come from \sim 2000 km distance.

Such data is now available from shuttle launches at Cape Canaveral as recorded at array station DLIAR at Los Alamos, New Mexico, and at array station Lac du Bonnet near Winnipeg, Canada, distances in the neighborhood of 2500 km. The energy released by the shuttles is approximately a kiloton of chemical explosive, released over the course of approximately 10 minutes as the shuttle rises from ground level to 50 km.

Figure 12 shows raw and filtered signals as recorded at the two sites, Figure 13 shows the signal and noise at DLIAR, and Figure 14 shows the signal and noise at Lac du Bonnet, Winnipeg.

We see that the best S/N is near 1 Hz at both stations. Analysis of the signals at DLIAR, following the procedures outlined in Blandford (2000), was distributed in an 04 November 1999 memorandum by Blandford (see Appendix). The memorandum concludes that the correlations near 1 Hz fit the Mack-Flinn model. McCormack (personal communication) analyzed the Lac du Bonnet data and also found correlation values near 1 Hz that fit the predictions of Mack-Flinn.

Blandford (2000) concluded that if the Mack-Flinn parameters were correct, and if S/N peaked near 1 Hz, that, then, 1 km was the optimum array aperture for both detection and location purposes.

Aperture and Side Lobes.

However, note that if processing is ideally performed near 1 Hz, that a 4-element, 1 km aperture array is undersampled in space; the wavelength at 1 Hz is approximately 0.35 km, but the closest spacing of elements is ~0.5 km.

As we have seen previously in this report, the large side lobes attendant on undersampling will lead to large values of correlation and F at those side lobes, so that detection and location processing using standard beamforming techniques will be difficult.

Of course, for high S/N and bandwidth, it will always be possible to select distinctive features on the time traces to determine relative delays and to determine the back azimuth of a plane wave. But to detect and locate weak signals, there is no alternative to beamforming in one of its many forms as an element in power detection, F detection, or average cross-correlation.

As seen before, the straightforward solution to this undersampling problem is to install a supplemental small aperture array together with the large aperture array.

Figure 15 shows the 1 Hz array response of DLIAR, a 4-element 1-km aperture array near Los Alamos to a signal arriving from the north at 0.33 km/sec. We see that there are many side lobes and conclude that signal processing using beamforming techniques would be extremely difficult.

Figure 16 shows the same array, but with the addition of a small (200 m aperture) subarray of three additional sensors to the southeast of DLI04. The side lobes are greatly reduced in number, and the peak relative power is 0.8 (2 dB down) instead of 0.9. This difference may be sufficient to resolve detection ambiguities, although a value of 0.5 (6 dB) would be desirable. More array response studies are needed.

How serious a problem are the side lobes in Figure 16? Figure 17 shows the response of the enhanced 7-element array at 0.5 Hz. There are some rather large side lobes with relative powers of 0.7 (3 dB). But note that these maxima are, of course, at different locations than the 1.0 Hz side lobes as seen in Figure 16. So, if the signal has a bandwidth of 0.5 to 1.0 Hz, most ambiguities should be resolvable since only on the main lobe will the peaks be in alignment.

It is worth noting the large number of beams required by these arrays for detection at 1 Hz. Requiring an overlap at the 2 dB contour, and covering velocities from 0.25 to 0.45 km/sec (plus a few beams near infinite velocity to catch seismically generated infrasound), the 1 km 7-element array requires approximately 300 beams. A 2 km aperture 7-element array would require perhaps 1200 beams. Compare these numbers to the requirement of only about 10 beams for an 0.2 km aperture 4-element array, similar to those historically deployed by Los Alamos.

One possible processing mode would be to detect only with the central four elements, and then locate using the full 7-element array, which will greatly improve accuracy. This sequential procedure would, however, lose about 2 dB in detection threshold over what could be obtained by processing the full array.

DETECTION ON SINGLE CHANNELS

Blandford (1981) evaluated the performance of several detector algorithms on single channels of signals buried in noise by plotting the detector's false alarm rate versus the number of detections. Since the signals were buried for a range of amplitudes, it was possible to transform the number of detections into a relative log-amplitude threshold scale in units of mb.

The best detector was found to be one in which the data were pre-filtered with the optimum filter (Freiberger, 1963), of the form $S/[N(S^2 + N^2)^{1/2}]$, where S is the signal amplitude spectrum adjusted in amplitude to be equal to or less than N at all frequency; *i.e.*, S just touches N from below.

Note that the above expression converges to the well-known S/N^2 form in the limit of small S. However, it is better to design the detector to be optimum at the amplitude value resulting in a S/N level where there is some chance of detection, instead of where there is no doubt, that the signal will be detected. It was found that the amplitude-adjusted filter was 0.02 mb better than the S/N^2 filter. (In the limit of large S, the optimum detector is $1/N$, a noise pre-whitening, or prediction-error, filter. This is obviously a limiting case of little interest, and was shown to be 0.25 mb inferior to the S/N^2 filter for low S/N events. Gjoystdal and Husebye (1972) reach a similar conclusion.)

The signal spectrum, S, is determined analytically as the product of a flat source spectrum appropriate for P for small events, times the instrument response, times a suitable attenuation. For P signals recorded at NORSAR, Blandford (1981) found the optimum attenuation t^* to be 0.0; for signals recorded at the Pinedale Wyoming array, the optimum t^* was 0.3.

The noise spectrum, N, may be directly calculated from the recorded data. It is important that this spectrum be very stable. Blandford (1981) showed that if it were averaged over only about 50 seconds, the spectrum was unstable and led to poor detection for a fixed false alarm rate. The noise spectrum must be continuously updated, like the LTA, but with a longer time constant. Just as the LTA must be protected from being distorted by signals, so must the smoothed noise spectrum.

At both NORSAR and Pinedale, the optimum STA averaging period was 10 seconds; it was ~0.05 mb units superior to 3 seconds. However, this large window may not be optimum for an array where loss of coherence, and thus S/N, often occurs a few seconds into the signal due to near-receiver scattering.

The optimum amplitude measure was found to be the square of the filtered data as contrasted to the absolute amplitude. This is fortunate because squaring is, of course, required for calculation of the F statistic. It was found that the difference was only about 0.01 mb units; this small value is compatible with similar small values found by Vanderkulk (1965) and others.

The optimum number of times to require that the detection statistic exceed the threshold in succession was found to be 1. This is in agreement with theoretical conclusions by Wirth *et al.* (1971, 1976).

For reasons not completely understood, the combination of the logZ statistic with the amplitude-adjusted $S/[N(S^2 + N^2)^{1/2}]$ optimum filter gave the best performance of all combinations tested.

It is important to realize that this detector performed better than did experienced analysts, so that it is impossible to use analysts as a test of the relative performance of detectors. Some other method must be used, such as signals buried in noise, or performing detection on single channels of events detected at arrays, as done by Blandford (1982).

SUGGESTIONS FOR DEVELOPMENT

The foregoing discussion makes it possible for us to outline a plan for development of the seismic and infrasound detection systems.

Seismic Detection System Development.

The first step would be to examine the existing deployment of coherent beams, to verify that one would expect coherent signals on those channels, and to verify that the assigned fixed frequency filters are appropriate. Then the STA/LTA detection algorithm on those channels can be replaced with an F detector, operating with a ≤ 10 -second STA. (As noted above, signal coherence at an array may degrade in a shorter time interval than 10 seconds; this will need to be examined. In that case, the STA should extend only over the time that the signal remains coherent. For example, it appears that for P waves at ARCESS from Novaya Zemlya, the 5 Hz signal passband where the S/N peaks remains coherent only for 1 second.)

Since ARCESS is an array identical in design to NORESS, whose beam deployment has been developed by expert workers from NORSAR as has been discussed in this report, ARCESS would be a plausible first array for which to modify the detection system.

The relative performance of this system can be evaluated by testing if it results in an increase in weak arrivals associated to analyst-verified large events, and if there are additional small-magnitude events created.

The next step in analysis would be to implement optimum filters in `beam_create` to replace the existing recursive fixed bandpass filters. This implementation will require some care. It is important to realize that on a beam, as contrasted to a single channel, the estimate for N should be performed using the noise on the beam, not on a single channel. The beam will have decreasing noise amplitude as frequency increases, as compared to the single channel. Also, some estimate of signal loss as a function of frequency should be made for each beam and implemented into the signal model, S .

The logZ statistic (Blandford, 1981; Shensa, 1977) should also be implemented with the optimum filter. Actually, logZ could be introduced at an intermediate step in order to ensure that each successive change behaves as expected and does not degrade performance. Each enhancement could be tested by the same means as above.

For each array, the system performance on regional signals should be evaluated, and incoherent beams deployed if the signals are incoherent at the appropriate phase and frequency.

Infrasound Detection System Development.

There is little question that the F detector is appropriate for infrasound detection. Since operations using standard digital beamforming are in their infancy, it seems suitable to begin with one of the existing on-line, 0.2 km aperture, 4-element arrays for which only a few beams are needed and for which there is no ambiguity due to side lobes.

The LSAR array would seem to be a good first selection, since it is nearly collocated with the 1-km aperture array DLIAR, and detections on the two systems may be compared.

The detector should be run over several days of LSAR data, perhaps using an 0.5 to 2.0 Hz prefilter, and an STA of a few minutes; its performance should be evaluated by analyst scanning of detections, and of the noise between detections.

A next study might be to evaluate a method of analyzing DLIAR as a spatially-aliased array; this capability may be needed if such arrays are installed. A suggested method is to form the many beams required to detect in the 0.5 to 2.0 Hz band, and then follow with an fk analysis which includes longer periods, perhaps extending to 0.2 Hz. The detections and azimuths may then be compared with those determined from LSAR to see if they are at least qualitatively correct.

In the cases where the longer period noise is well-defined and propagating, as is presumably the case in Figure 14, where the Lac du Bonnet noise near 0.2 Hz is presumably microbaroms, the DLIAR azimuth estimates should be enhanced by running the multiple signal “stripping” model discussed by Mack and Smart (1973), and the exact multi-signal fk processor recently developed by Smart, personnel communication (2000).

Further development would include optimum S/N²-type filters, and a channel-mean-square-weighted F statistic approach as suggested by Shumway (personal communication). This latter capability will enable detection even if there is high noise on two of the four channels. This is a capability greatly to be desired in infrasound systems where there are likely to be only four channels installed, and where it is common for wind noise conditions to be substantially different on different channels.

FIGURES

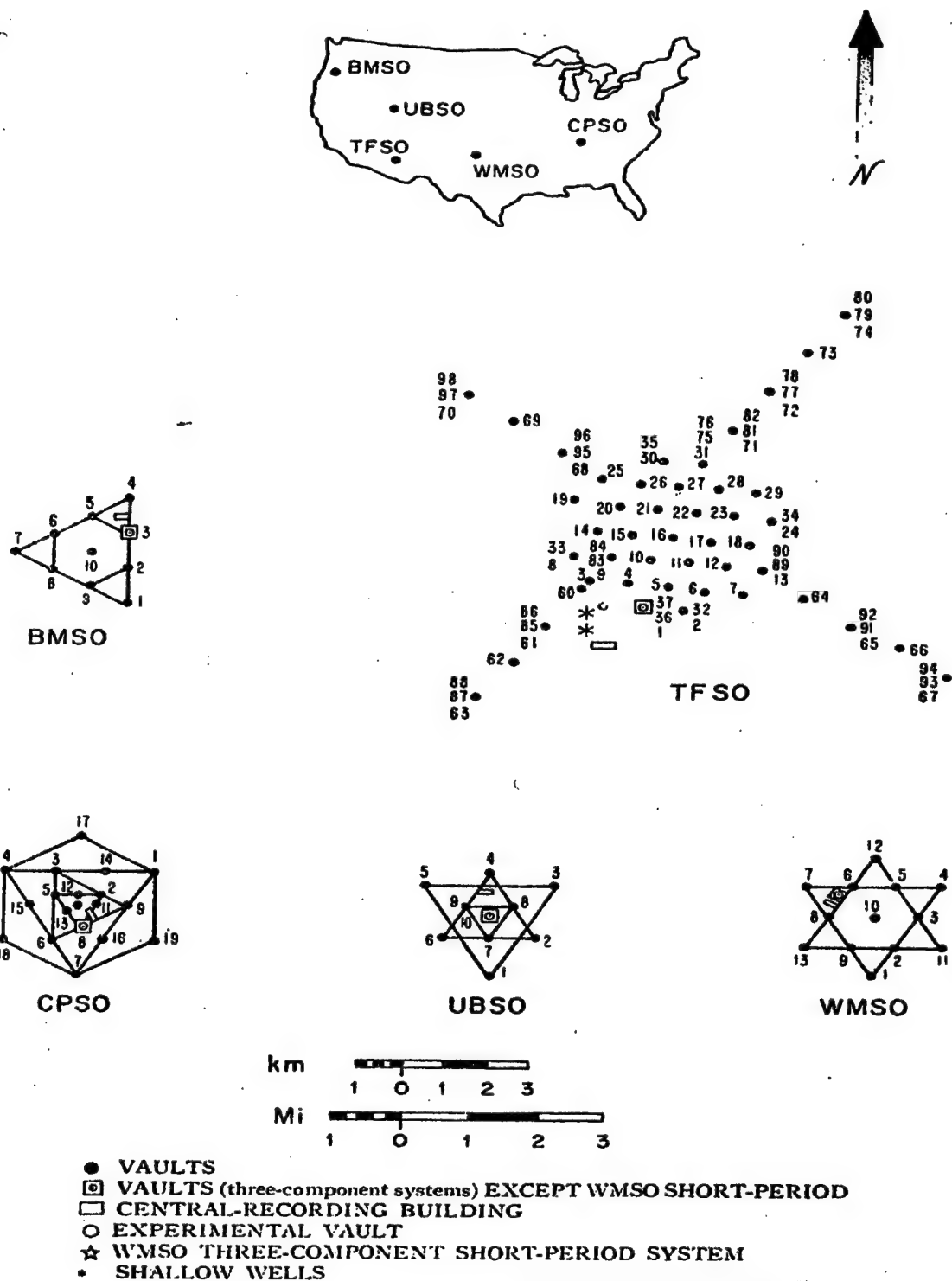


Figure 1. Configuration of the early Geneva-type observatories: Blue Mountain, Cumberland Plateau, Uinta Basin, Tonto Forest, and Wichita Mountain Seismic Observatories

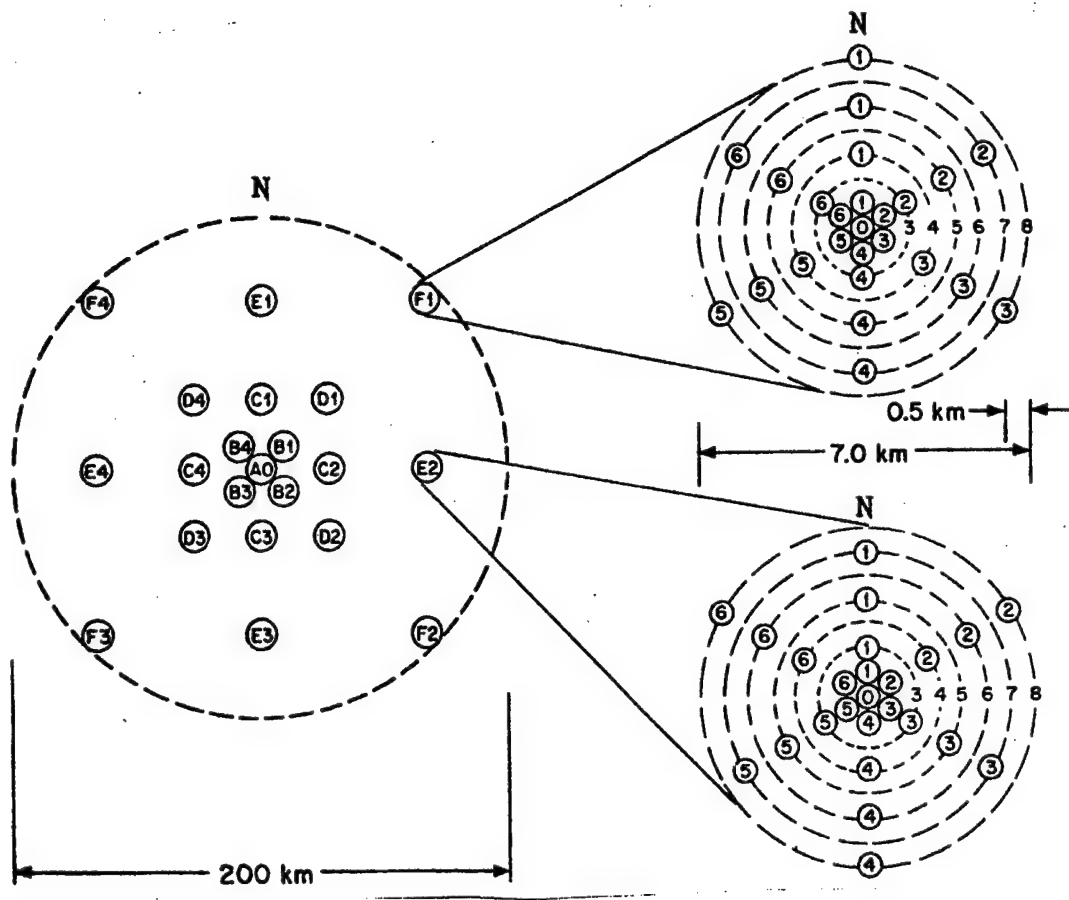


Figure 2. Configuration of early LASA design. LASA was installed in Montana with the center of the A0 subarray at 46.6886°N , 106.2222°W . It was operational between 1966 and 1978. Communication headquarters was in Billings, Montana.

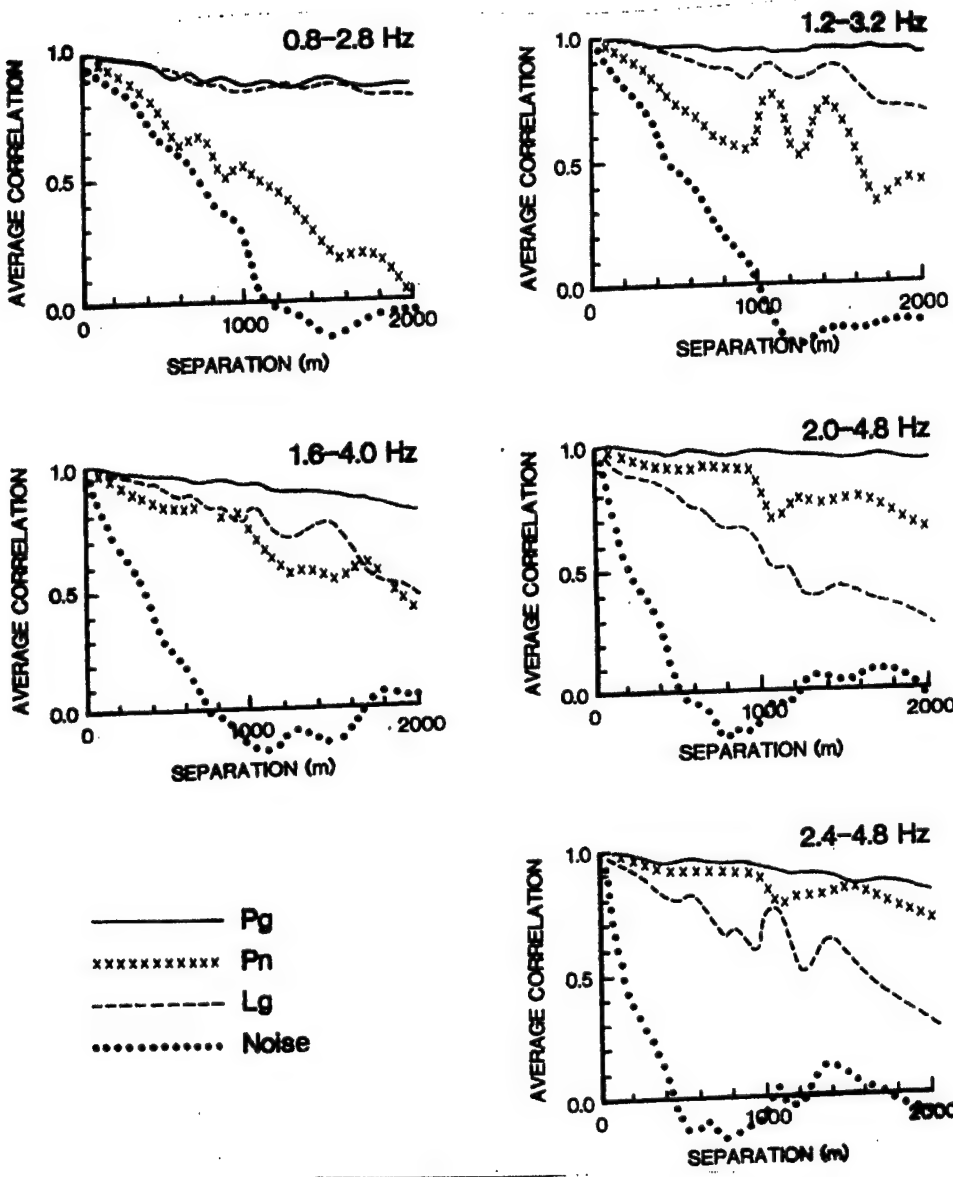


Figure 3. Signal and noise correlation estimates from a temporary array deployed near the NOR-ESS site (60.735°N , 11.541°E) (from Mykkeltveit *et al.* (1983)). Correlation versus distance for Pg, Pn, Lg, and noise for the five frequency ranges indicated. Each curve is based on measurements from 66 combinations of sensor pairs. For bandpasses with lower limits near 1 Hz, the noise correlation passes through 0.0 near 1.0 km. For bandpasses with lower limits above 2 Hz, the noise correlation passes through zero near 0.4 km. These results are corroborated by results reported by Harjes (1990) in Germany, whereas signal correlation reported by Harjes is generally higher

NORESS

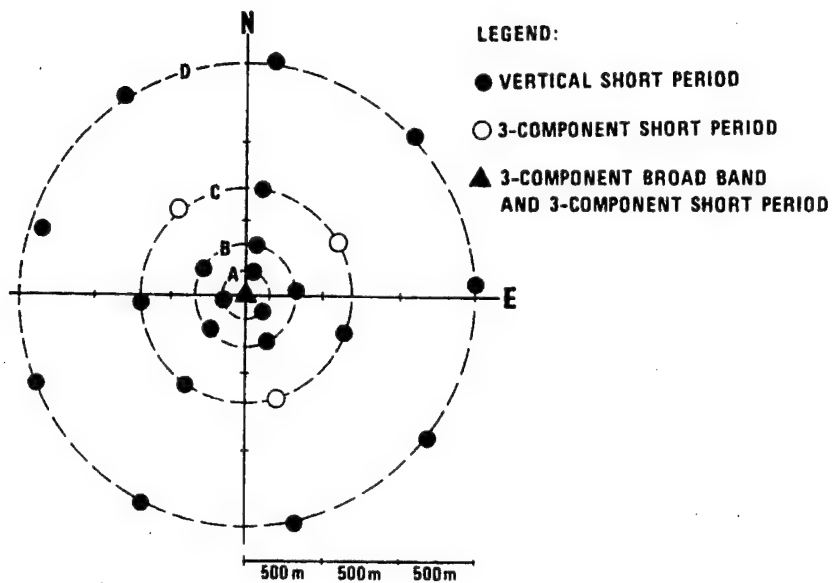


Figure 4. The geometry of the NORESS array. The inner ring, A, is deployed at a radius of $R_{min}=150$ m. Successive rings are at radii of successive factors of $\alpha = 2.15$ so that the D ring is at a radius of 1.491 km, giving an array aperture of approximately 3 km.

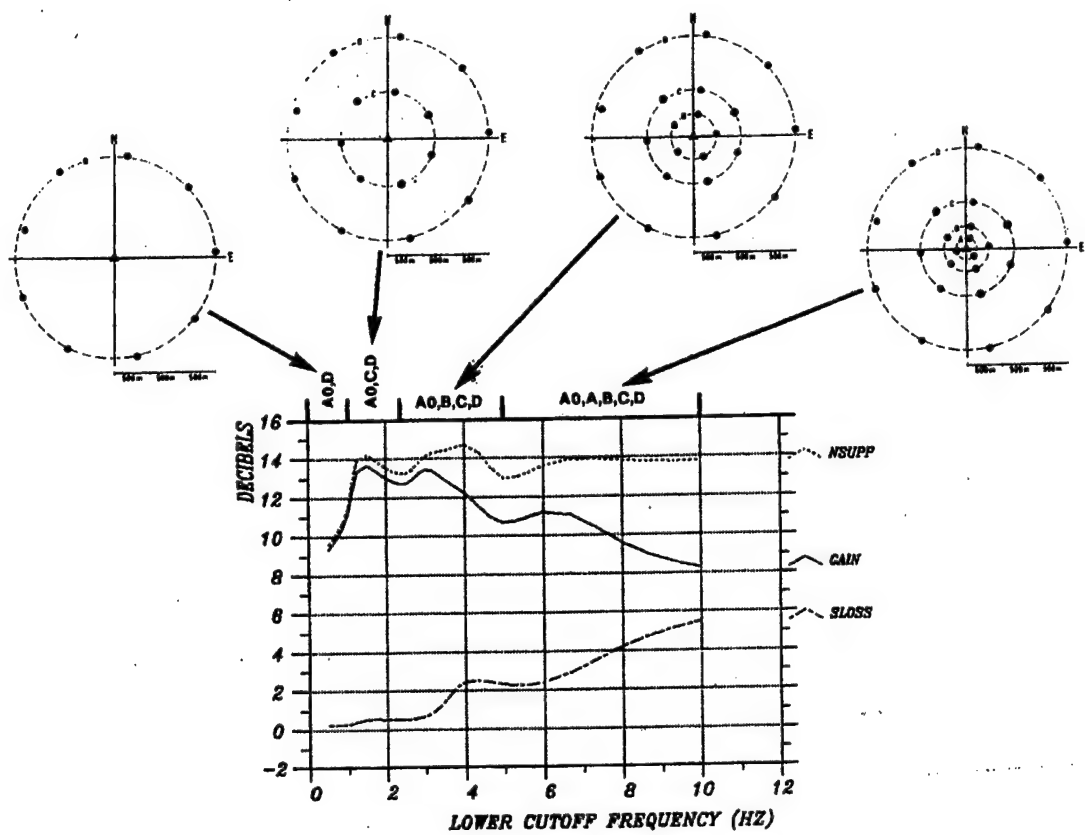


Figure 5. Gain curve (from Kvaerna, 1989) representing the best gain values produced by any of 10 NORESS subgeometries tried. In addition, there is plotted the corresponding noise suppression (NSUPP) and signal loss (SLOSS).

NORESS BEAM DEPLOYMENT

Beam	Velocity	Azimuth	Filter Band	Threshold	Configuration
N011	99999.9	0.0	0.5- 1.5	4.0	D
N021	99999.9	0.0	1.0- 3.0	4.0	CD
N031	99999.9	0.0	1.5- 3.5	4.0	CD
N032-037	11.0	*	1.5- 3.5	4.0	CD
N038	15.8	80.0	1.5- 3.5	3.5	CD
N039	10.0	30.0	1.5- 3.5	3.5	CD
N041	99999.9	0.0	2.0- 4.0	4.0	CD
N042-047	10.2	*	2.0- 4.0	4.0	CD
N048	15.8	80.0	2.0- 4.0	3.5	CD
N049	10.0	30.0	2.0- 4.0	3.5	CD
N051	99999.9	0.0	2.5- 4.5	4.0	BCD
N052-057	8.9	*	2.5- 4.5	4.0	BCD
N058	15.8	80.0	2.5- 4.5	3.5	BCD
N059	10.0	30.0	2.5- 4.5	3.5	BCD
N061	99999.9	0.0	3.0- 5.0	4.0	BCD
N062-067	10.5	*	3.0- 5.0	4.0	BCD
N068	15.8	80.0	3.0- 5.0	3.5	BCD
N069	10.0	30.0	3.0- 5.0	3.5	BCD
N071	99999.9	0.0	3.5- 5.5	4.0	BC
N072-077	11.1	*	3.5- 5.5	4.0	BC
N081	99999.9	0.0	4.0- 8.0	4.0	BC
N082-087	9.5	*	4.0- 8.0	4.0	BC
N091	99999.9	0.0	5.0-10.0	4.5	BC
N092-097	10.5	*	5.0-10.0	4.5	BC
N101	99999.9	0.0	8.0-16.0	4.5	AB
N102-107	9.9	*	8.0-16.0	4.5	AB
NH01	99999.9	0.0	2.0- 4.0	2.4	ne
NH02	99999.9	0.0	3.5- 5.5	2.4	ne
NH03	99999.9	0.0	5.0-10.0	2.4	ne
NH04	99999.9	0.0	8.0-16.0	2.5	ne
NV01	99999.9	0.0	0.5- 1.5	2.5	D
NV02	99999.9	0.0	1.0- 2.0	2.5	C
NV03	99999.9	0.0	1.5- 2.5	2.5	C
NV04	99999.9	0.0	2.0- 3.0	2.5	C
NV05	99999.9	0.0	2.0- 4.0	2.4	C
NV06	99999.9	0.0	3.5- 5.5	2.4	C

Figure 6. NORESS Beam Deployment Table. The table gives name of beam, steering velocity (in km/sec), steering azimuth (in degrees), filter band (in Hz), STA/LTA threshold, and subconfiguration (in terms of which rings are included; the sensor at the central site, A0, participates in all beams). The NH01-04 beams are incoherent and use the eight horizontal channels (ne in the table, for north-south and east-west) of the stations at A0, C2, C4, and C7. The NV01-06 beams are also incoherent, and use vertical sensors as indicated. The remaining beams are conventional, coherent ones, using vertical channels only. The six coherent beams N032-N037 are identical except for steering azimuths, which have values of 30°, 90°, 150°, 210°, 270°, and 330°, respectively. The same pattern repeats for other coherent beams further down the table and is indicated by an asterisk in the azimuth column. Four special coherent beams are steered toward each of the test sites at Semipalatinsk and Novaya Zemlya (at azimuths of 80° and 30°, respectively).

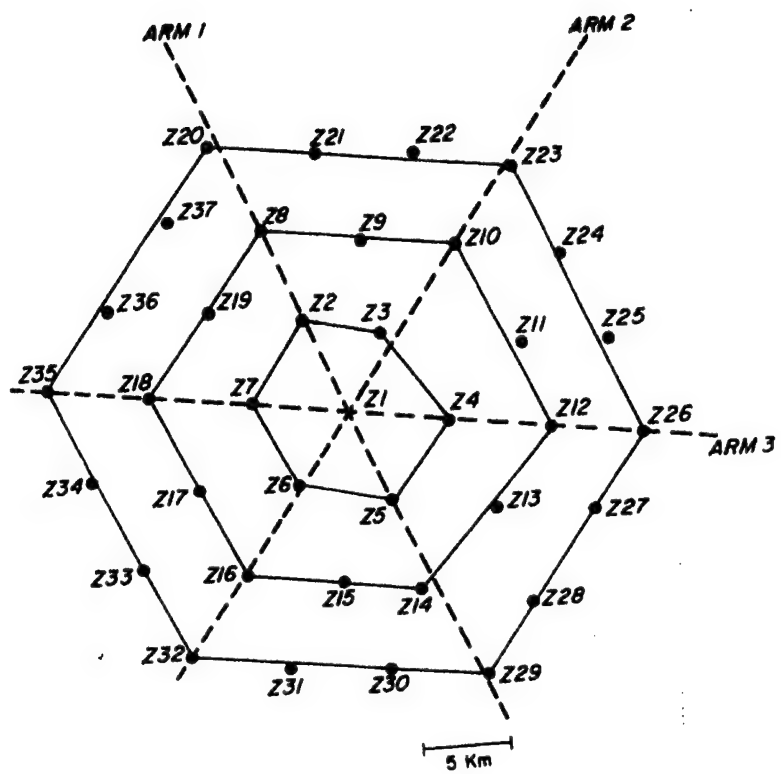


Figure 7. TFSO 37-element array in Arizona. Elements 3, 5, 7, 8, 12, and 16 were not used in the F detector.

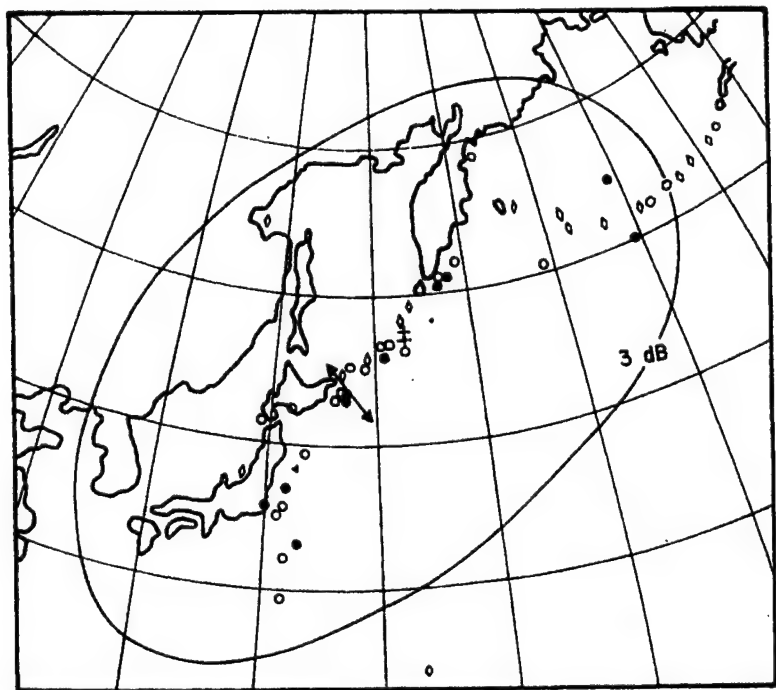


Figure 8. 3 dB contour of the short-period TFSO Kurile beam.

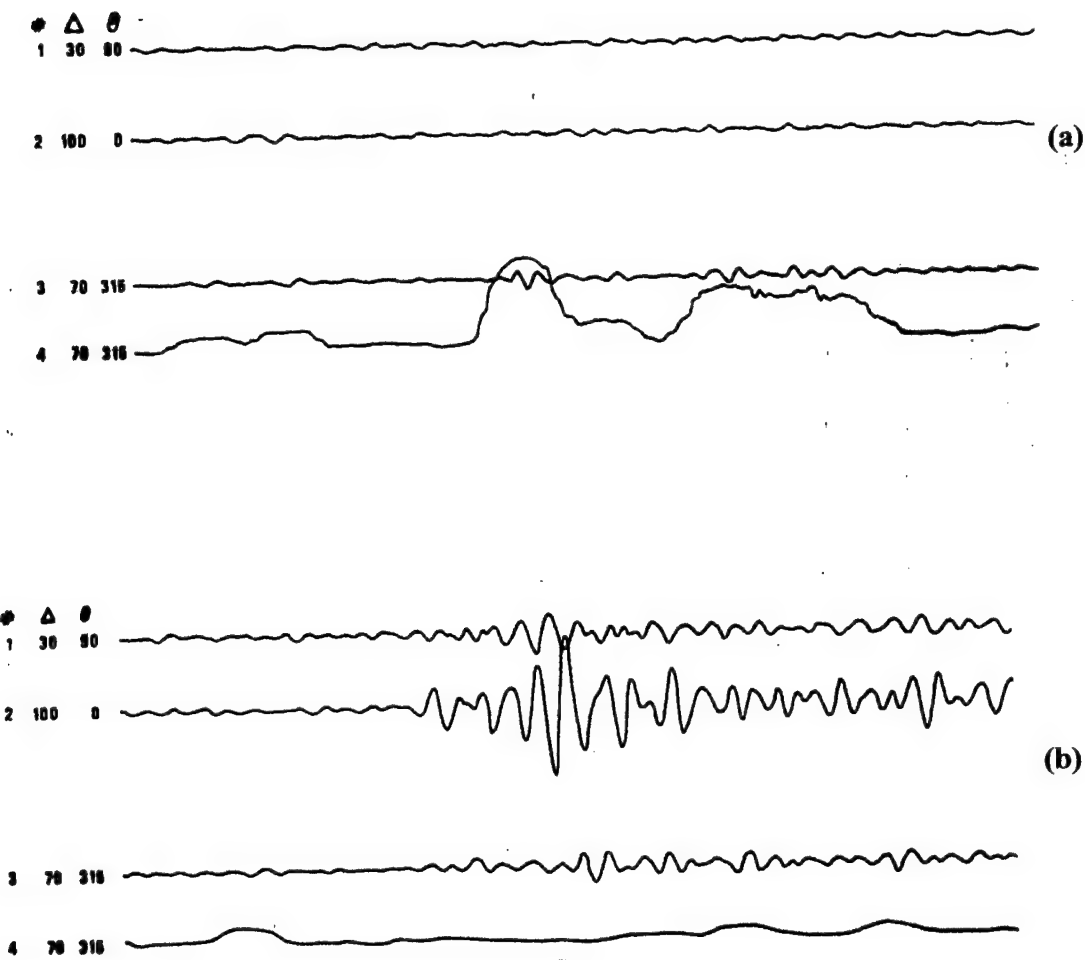
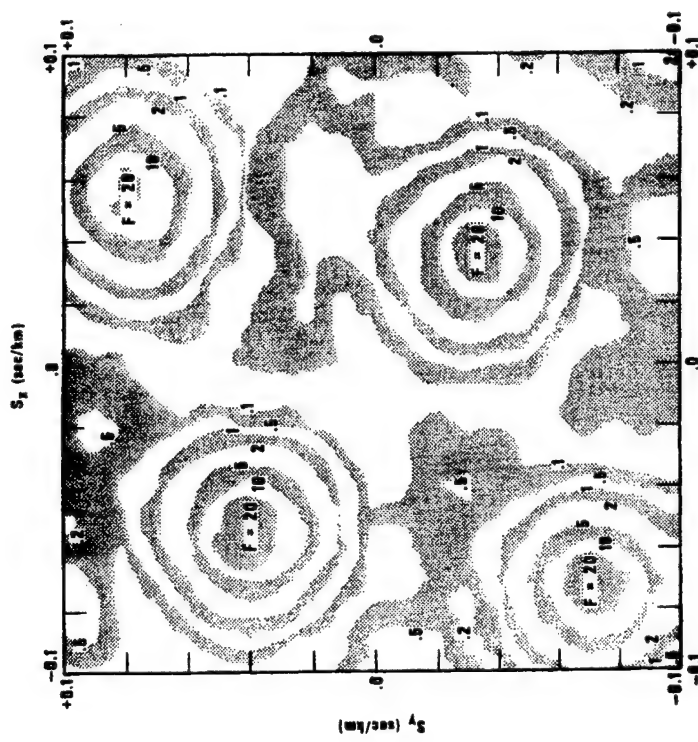


Figure 9. Detector response traces. (a) The upper four traces show detector response on 0732, 25 April 1970. Trace 3 shows the Kurile beam through the 0.5-1.5 Hz filter. Trace 4 is the detector operating on trace 3. (b) The lower four traces show the detector response on 1343, 19 April 1970, to off-beam event. Trace 3 shows the Kurile beam through the filter in Figure 3. Trace 4 is the detector operating on trace 3.

(b)



(a)

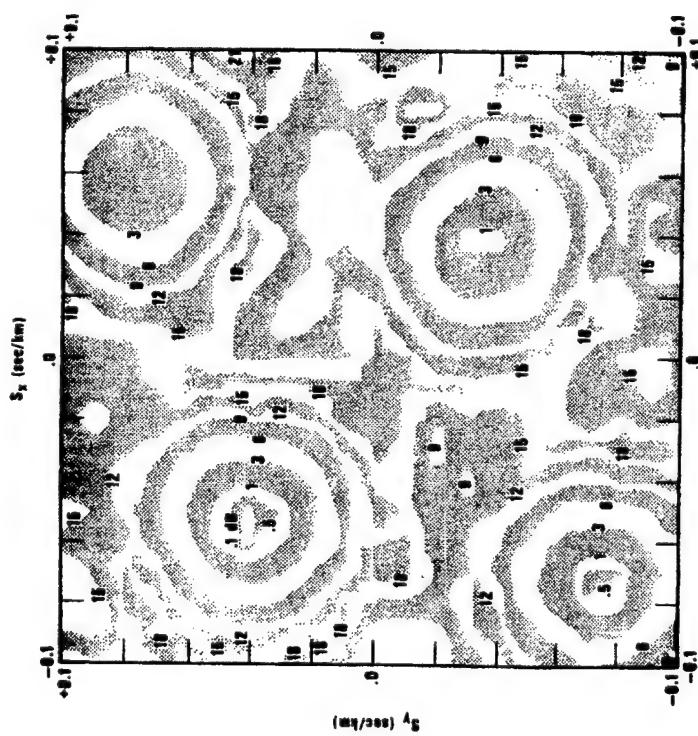
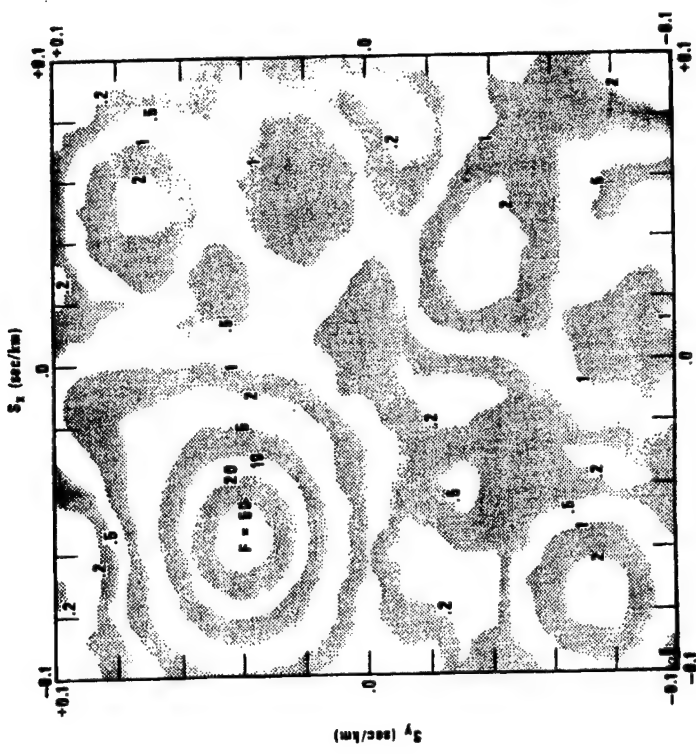


Figure 10. (a)(b) Power-slowness and F plots of a Fox event as seen by elements 1, 8, 10, 12, 14, 16, and 18 of TFSO, the center element and every other sensor in the second ring, resulting in a minimum spacing of 10 km (see Figure 7).

(b)



(a)

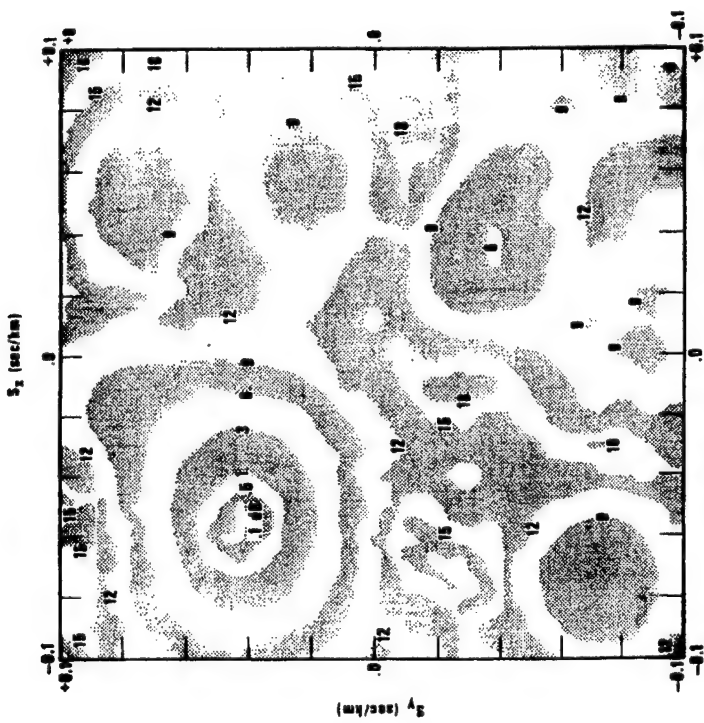


Figure 11. (a)(b) Power-slowness and F plots of the Fox event as seen by the TFSO elements in Figure 10a,b plus elements 3, 4, and 5. This results in the addition of a relatively small, 5 km spacing subarray which greatly reduces the overall array side lobes.

Shuttle Signals at Los Alamos (DLI04) and Winnipeg (ISM1)

A

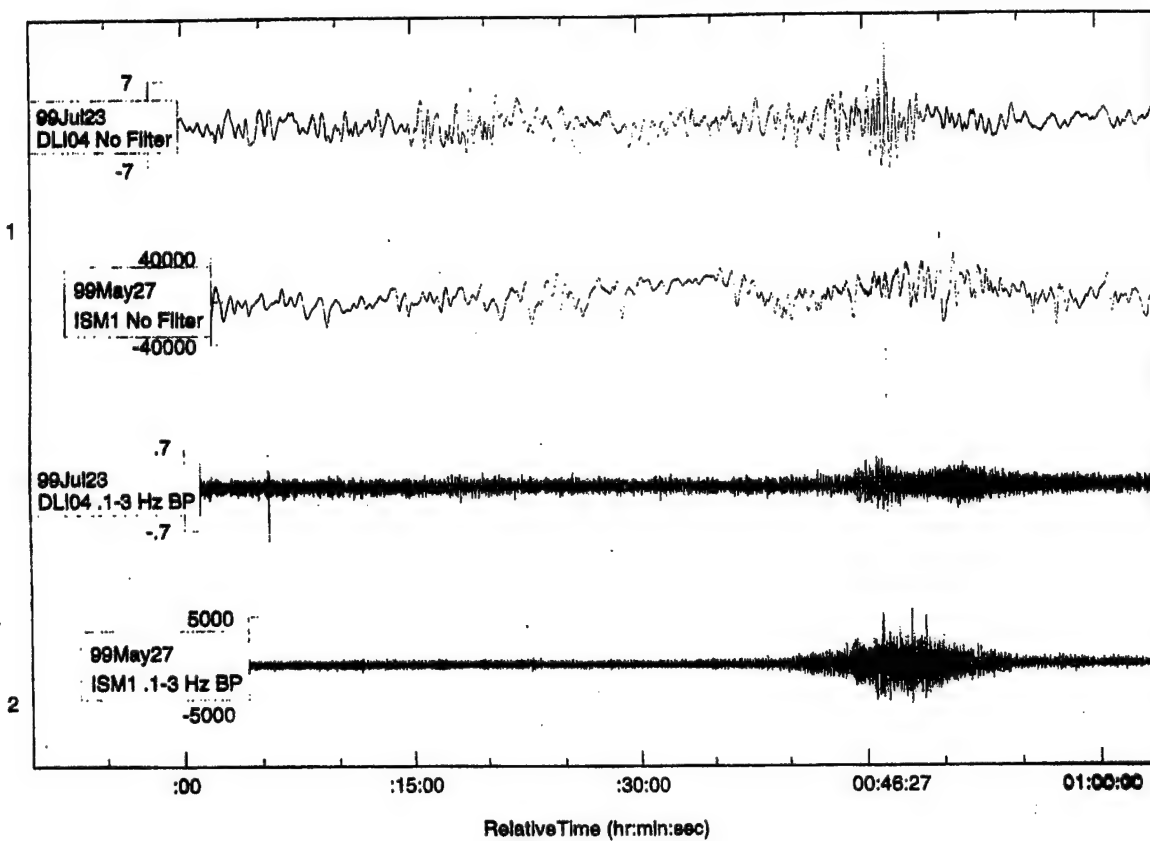


Figure 12. Raw and filtered traces of two shuttle launches: 23 July 1999, observed at DLIAR; and 27 May 1999, observed at Lac du Bonnet, Winnipeg. The signal has approximately a 10-minute duration and the peak amplitude arrives near the vertical line.

Los Alamos DLI04 S/N for 23 July 1999 Shuttle Launch

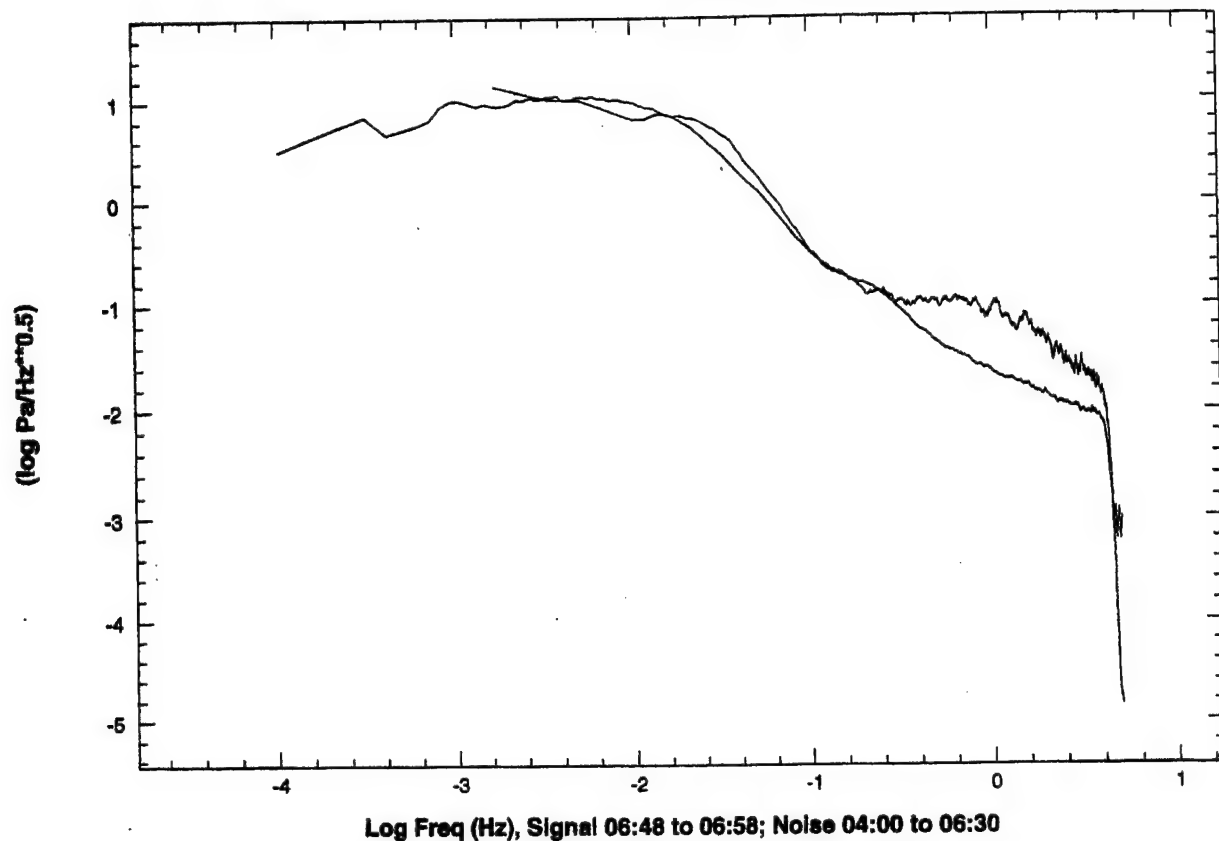


Figure 13. Signal and noise spectra of the DLIAR 23 July 1999 shuttle signal. We see that the peak in S/N is near 1 Hz. At the low-frequency end, the signal is cut off by rising noise.

Winnipeg ISM1 S/N for 27 May 1999 Shuttle Launch

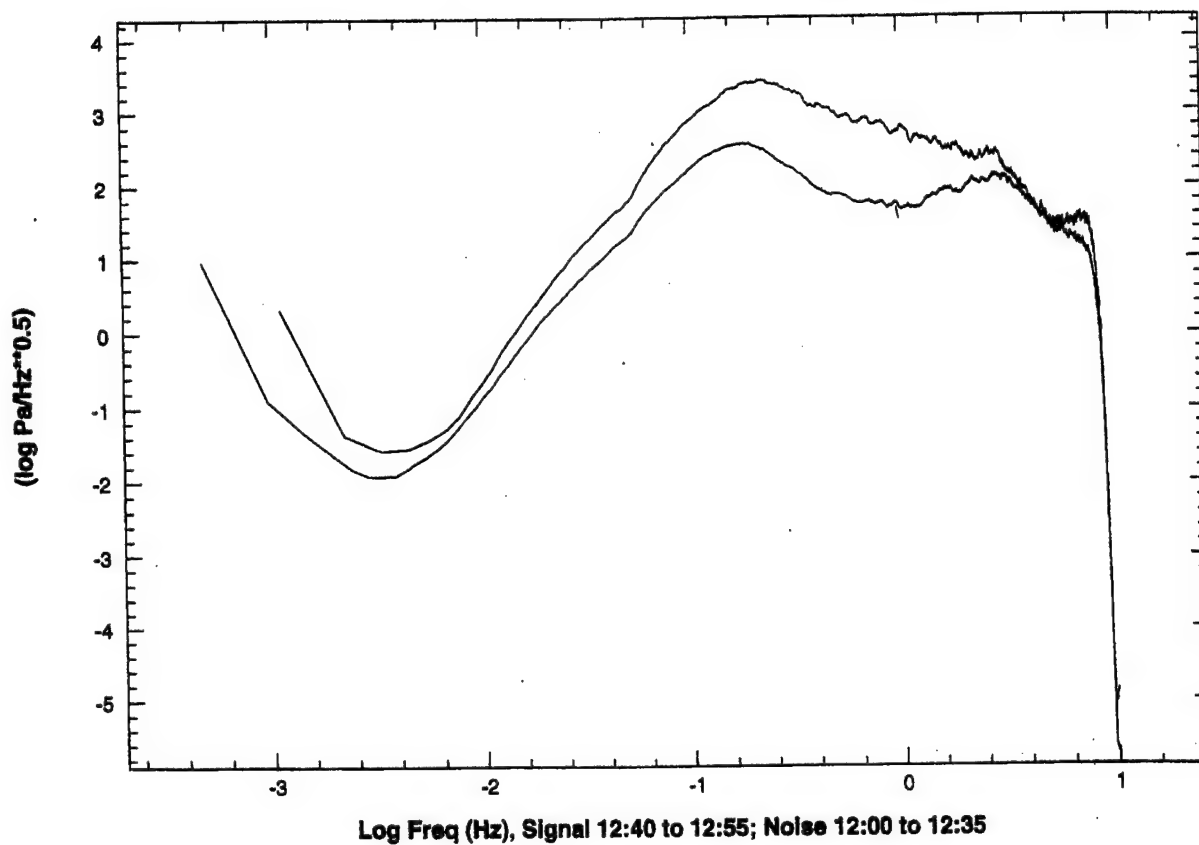


Figure 14. Signal and noise spectra for the Lac du Bonnet 27 May 1999 shuttle signal. We see that the peak in S/N is slightly lower than 1 Hz, but that good S/N extends to approximately 0.2 Hz because the noise spectrum is uncharacteristically flat, revealing the microbarom peak.

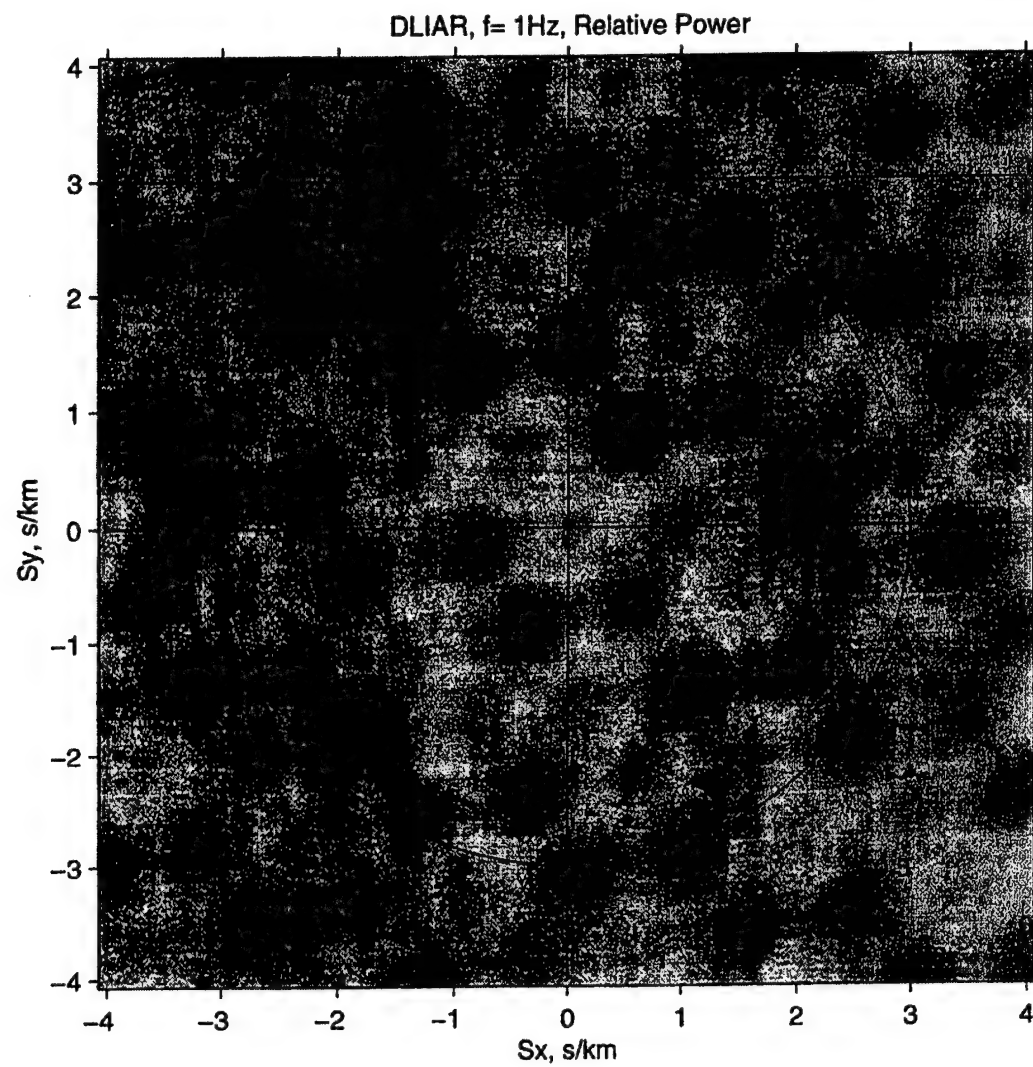


Figure 15. Wavenumber 1 Hz power spectrum of the DLIAR array for a signal arriving from the north at 0.33 km/sec. We see multiple side lobes with relative amplitude of 0.9 or greater. An array response of this sort portends grave difficulties in array processing.

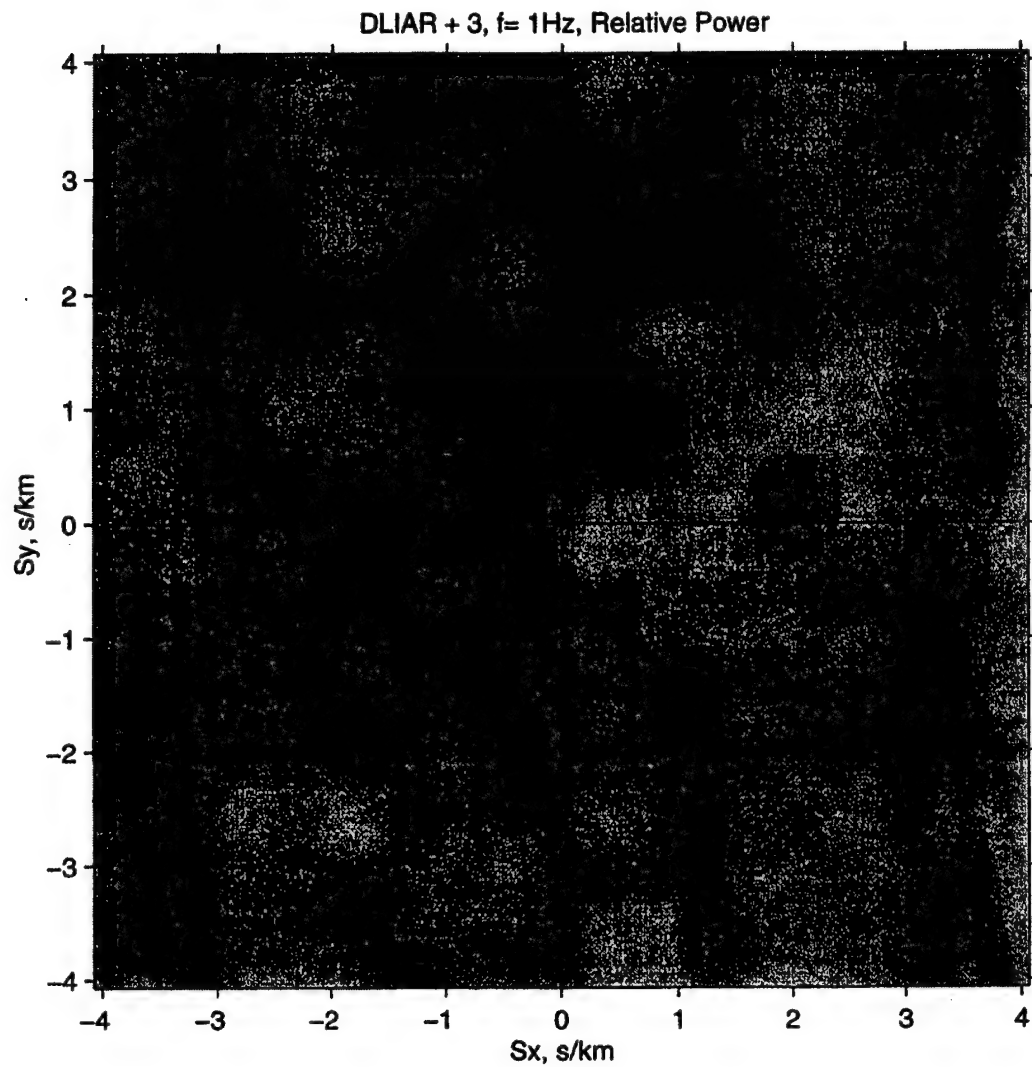


Figure 16. Wavenumber 1 Hz power spectrum of the augmented DLIAR array to a signal arriving from the north at 0.33 km/sec. The array is augmented by three additional sensors to the southeast of DLI04, forming a 200-meter aperture 4-element subarray. This array response is much better than that in Figure 15, but further analysis is warranted.

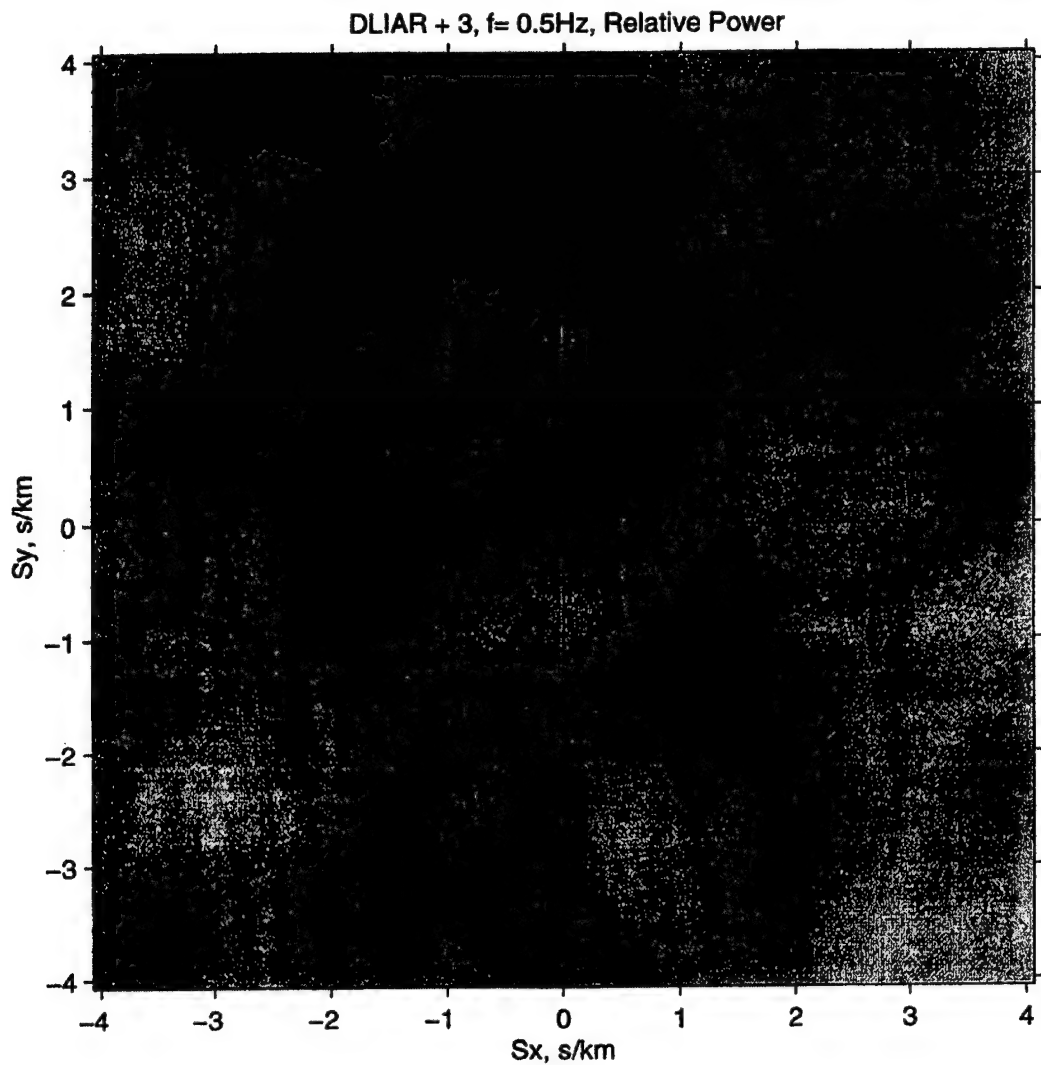


Figure 17. Wavenumber 0.5 Hz power spectrum of the augmented DLIAR array to a signal arriving from the north at 0.33 km/sec. The array is augmented by three additional sensors to the southeast of DLI04, forming a 200-meter aperture 4-element subarray. The lack of side lobe overlap between this response and the previous one for 1 Hz suggests that an 0.5-1.0 Hz signal might have few side lobe problems.

REFERENCES

- Bedard, A.J., and D.M. Caldwell (1970). Instructions for the operation of correlator-analyzer N4: ESSA Technical Manual ERL 2, ESSA TM ERL 2, US Department of Commerce.
- Blandford, R.R. (2002). Detection and azimuth estimation by infrasonic arrays as a function of array aperture and signal coherence, AFTAC-TR-02-005.
- Blandford, R.R. (1997). Design of infrasonic arrays, AFTAC-TR-97-013.
- Blandford, R.R. (1982). Single channel seismic event detection on Alaskan short-period data, VSC-TR-82-3, Teledyne Geotech, Alexandria, Virginia.
- Blandford, R.R. (1981). Single channel seismic event detection, VSC-TR-81-8, Teledyne Geotech, Alexandria, Virginia.
- Blandford, R.R., and D.M. Clark (1975). A note on seismic array design.
- Blandford, R.R. (1974). An automatic event detector at the Tonto Forest seismic observatory, *Geophysics*, **39**, 633-643.
- Blandford, R.R. (1972). Qualitative properties of the F-detector, *Seismic Data Laboratory Report No. 291*, Teledyne Geotech, Alexandria, Virginia. AD 753 059.
- Blandford, R.R., and D.M. Clark (1971). Seismic Array Design, *Seismic Data Laboratory Report No. 267*, Teledyne Geotech, Alexandria, Virginia.
- Brown, R.F. (1963). An automatic multichannel correlator, *J. Res., Nat. Bur. Stand.*, **67C**, 33-38.
- Capon, J., R.J. Greenfield, R.J. Kolker, and R.T. Lacoss (1968). Short-period signal processing results for the Large Aperture Seismic Array, *Geophysics*, **33**, 452-472.
- Carpenter, E.W. (1965). An historical review of seismometer array development, *Proceedings of the IEEE*, **53**, 1816-1821.
- Der, Z., M.E. Marshall, A. O'Donnell, and T.W. McElfresh (1984). Spatial coherence structure and attenuation of the Lg phase, site effects, and interpretation of the Lg coda, *Bull. Seism. Soc. Am.*, **74**, 1125-1148.
- Flatte, S.M., and R. Wu (1988). Small-scale structure in the lithosphere and asthenosphere deduced from arrival time and amplitude fluctuations at NORSAR, *J. of Geoph. Res.*, **93**, 6601-6614.
- Followill, F., and D. Harris (1983). Comments on small aperture array designs. Informal Report, Lawrence Livermore National Laboratory.

- Freiberger, W.F., (1963). An approximate method in signal detection, *Quarterly J. App. Math.*, **20**, 373-378.
- Frosh, R.A., and P.E. Green (1966). The concept of a large aperture seismic array, *Proc. Royal Soc., A*, **290**, 368-384.
- Gjoystdal, H., and E.S. Husebye (1972). A comparison of performance between prediction error and bandpass filters, *NORSAR Technical Report 48*, Royal Norwegian Council for Scientific and Industrial Research, Kjeller, Norway.
- Green, P.E. (1965). A large aperture seismic array, Lincoln Labs, *Seismic Discrimination Group Report 1965-1*, ESD-TDR-65-26.
- Green, P.E., R.A. Frosh, and C.F. Romney (1965). Principles of an experimental Large Aperture Seismic Array (LASA), *Proc. IEEE*, 1831-1833.
- Harjes, H.P. (1990). Design and siting of a new regional seismic array in Central Europe, *Bull. Seism. Soc. Am.*, **80**, 1801-1817.
- IBM (1972). Seismic array design handbook: Contract F119628-68-C-400, Fed. Syst. Div., IBM, Gaithersburg, MD.
- Katz, C.N., D.J. Brown, and J. Wang (1999). Infrasonic detection and feature extraction and the relationship between F-statistic and mean normalized cross-correlation, American Geophysical Union, 01-04 June 1999, Boston, Massachusetts.
- Kvaerna, T. (1989). On exploitation of small-aperture NORESS type arrays for enhanced P-wave detectability, *Bull. Seism. Soc. Am.*, **79**, 888-900.
- Kvaerna, T., S. Kibsgaard, and F. Ringdal (1987). False alarm studies and threshold determination for regional event detection. *Semiannual Tech. Summary, 1 April-30 September 1987*, NORSAR Sci. Rept. No. 1-87/88, Kjeller, Norway.
- Kvaerna, T., and D.J. Doornbos (1986). An integrated approach to slowness analysis with arrays and three-component stations, *Semiannual Tech. Summary, 1 October 1985-31 March 1986*, NORSAR Sci. Rept. No. 2-85/86, Kjeller, Norway.
- Lacoss, R.T. (1972). Variation of false alarm rates at NORSAR, *Seismic Discrimination, Semiannual Technical Summary*, June 1972, 53-57, Lincoln Lab., Mass. Inst. of Tech., Cambridge, Massachusetts.
- Mack, H., and E. Smart (1973). Automatic processing of multi-array long-period seismic data, *Geophys. J. R. astr. Soc.*, **35**, 215-224.
- Mack, H., and E. Smart (1972). Frequency domain processing of digital microbarograph array data, *J. Geoph. Res.*, **77**, 490.

- Mack, H., and E.A. Flinn (1971). Analysis of the spatial coherence of short-period acoustic-gravity waves in the atmosphere, *Geophys. J. R. Astr. Soc.*, **26**, 255-269.
- Melton, Ben S., and Leslie F. Bailey (1957). Multiple Signal Correlators, *Geophysics*, v. XXII, No. 3, pp. 565-588.
- Mrazek, C.P., Z.A. Der, B.W. Barker, and A. O'Donnell (1980). Seismic array design for regional phases, in *Studies of Seismic Wave Characteristics at Regional Distances*, AL-80-1, Teledyne Geotech, Alexandria, Virginia.
- Mykkeltveit, S., F. Ringdal, T. Kvaerna, and R.W. Alewine (1990). Application of regional arrays in seismic verification, *Bull. Seism. Soc. Am.*, **80**, Part B, 1777-1800.
- Mykkeltveit, S. (1985). A new regional array in Norway: design work and results from analysis of data from a provisional installation, in *The VELA Program: A Twenty-Five Year Review of Basic Research*. A.U. Kerr, Editor, Defense Advanced Research Projects Agency.
- Mykkeltveit, S., and H. Bungum (1984). Processing of regional seismic events using data from small aperture arrays, *Bull. Seism. Soc. Am.*, **74**, 2313-2333.
- Mykkeltveit, S., K. Astebol, D.J. Doornbos, and E.S. Husebye (1983). Seismic array configuration optimization, *Bull. Seism. Soc. Am.* **73**, 173-186.
- Ringdal, R., E.S. Husebye, and A. Dahle (1975). P-wave envelope representation in event detection using array data, in *Exploitation of Seismograph Networks*, K.G. Beauchamp, Editor, Noordhoff-Leiden.
- Ringdal, F., E.S. Husebye, and A. Dahle (1972). Event detection problems using a partially coherent seismic array, *NORSAR Technical Report 45*, Royal Norwegian Council for Scientific and Industrial Research, Kjeller, Norway.
- Shensa, M.J. (1977). The deflection detector, its theory and evaluation on short-period seismic data, TR-77-03, Texas Instruments, Alexandria, Virginia.
- Shumway, R.H., S. Kim, and R.R. Blandford (1999). Nonlinear estimation for time series observed on arrays, in *Asymptotics, Nonparametrics, and Time Series*, S. Ghosh, Editor, Marcel Dekker.
- Shumway, R.H. (1988). *Applied Statistical Time Series Analysis*, Prentice Hall.
- Shumway, R.H. (1971). On detecting a signal in N stationarily correlated noise series: *Technometrics*, **13**, no. 3, 499-519.
- Shumway, R.H. (1970). Applied regression and analysis of variance for stationary time series: *J. Am. Stat. Assn.*, **65**, 1927-1946.

Smart, E., and Flinn, E.A. (1971). Fast frequency wavenumber analysis and Fisher signal detection in real time infrasonic array processing, *Geophys. J. R. astr. Soc.*, **26**, 279-284.

Vanderkulk, W., F. Rosen, and S. Lorenz (1965). Large aperture seismic array signal processing study, *IBM Final Report*, ARPA Contract SD-296, 15 July 1965.

Wahl, D. (1996b). User's manual for the Detection and Feature Extraction program (DFX), SAIC-96/1098, Science Applications International Co., Geophysical Systems Operation, San Diego, California.

Wahl, D. (1996a). Programmers guide for the Detection and Feature Extraction program (DFX), SAIC-96/1069, Science Applications International Co., Geophysical Systems Operation, San Diego, California.

Wirth, M.H., R.R. Blandford, and R.H. Shumway (1976). Automatic seismic array and network detection: *Bull. Seism. Soc. Am.*, **66**, no. 4, 1375-1380.

Wirth, M.H., R.R. Blandford, and R.H. Shumway (1971). Automatic network detection. *Seismic Data Laboratory Report No. 285*, Teledyne Geotech, Alexandria, Virginia, AD 737 129.

DISTRIBUTION

California Institute of Technology
ATTN: Prof. Thomas Ahrens
Seismological Laboratory, 252-21
Pasadena CA 91125

Air Force Research Laboratory/VSBL
ATTN: Dr. Robert Raistrick
29 Randolph Rd.
Hanscom AFB MA 01731-3010

OATSD(NCB)/NT
ATTN: Mr. Patrick Wakefield
1515 Wilson Blvd., Suite 720
Arlington VA 22209

Pennsylvania State University
ATTN: Prof. S. Alexander & Prof. C. Langston
Department of Geosciences
537 Deike Building
University Park PA 16802

University of Colorado
ATTN: Prof. C. Archambeau, Prof. D. Harvey,
Dr. Anatoli Levshin, & Prof. M. Ritzwoller
Department of Physics/JSPC
3100 Marine Street
Boulder CO 80309-0583

Cornell University
ATTN: Prof. M. Barazangi
Institute for the Study of the Continents
Department of Geological Sciences
3126 SNEE Hall
Ithaca NY 14853

State University of New York, Binghamton
ATTN: Prof. F.T. Wu
Department of Geological Sciences
Binghamton NY 13901

ENSCO, Inc./APA Division
ATTN: Dr. D.R. Baumgardt & Dr. Z. Der
5400 Port Royal Road
Springfield VA 22151-2388

University of Arizona
ATTN: Dr. S. Beck & Prof. T.C. Wallace
Department of Geosciences
Gould Simpson Building
Tuscon AZ 85721

Maxwell Technologies, Inc.
ATTN: Dr. T.J. Bennett & Mr. J. Murphy
Geophysics & Resource Technologies Group
11800 Sunrise Valley Drive, Suite 1212
Reston VA 22091

University of California, San Diego
ATTN: Dr. J. Berger, Dr. L. Burdick,
Dr. M. Hedlin, Prof. B. Minster,
Prof. J.A. Orcutt, & Dr. F.L. Vernon
Scripps Institution of Oceanography
Institute of Geophysics and Planetary Physics
9500 Gilman Dr.
La Jolla CA 92093

US Department of Energy
ATTN: Ms. Leslie A. Casey
NNSA/NA-22
1000 Independence Ave., SW
Washington DC 20585-0420

Multimax, Inc.
ATTN: Dr. W. Chan, Dr. I.N. Gupta,
& Mr. W. Rivers
1441 McCormick Drive
Largo MD 20774

Virginia Polytechnical Institute
ATTN: Dr. M. Chapman
Seismological Observatory
Department of Geological Sciences
4044 Derring Hall
Blacksburg VA 24061-0420

US Department of State
AC/VC
ATTN: Dr. M. Dreicer, Dr. C. Yeaw,
Dr. W. Leith, & Mr. R. Morrow
2201 C Street, N.W.
Washington DC 20520

University of Connecticut, Storrs
ATTN: Prof. V.F. Cormier
Department of Geology & Geophysics
U-45, Room 207
Storrs CT 06269-2045

DTRA/TDAS
ATTN: Dr. Anton Dainty, Dr. Jay Davis, &
Dr. R.A. Gustafson
8725 John J. Kingman Rd., MS6201
Ft. Belvoir VA 22060

DTRA/OSTN
ATTN: Dr. C. Gallaway & Dr. R. Goodwin
6801 Telegraph Rd.
Alexandria VA 222310

DTRA/CP
ATTN: Dr. Hopkins
6801 Telegraph Rd.
Alexandria VA 222310

Defense Technical Information Center
8725 John J. Kingman Road, Suite 0944
Ft. Belvoir VA 22060-6218

University of California, San Diego
ATTN: Dr. Catherine de Groot-Hedlin
Institute of Geophysics & Planetary Sciences
8604 La Jolla Shores Drive
San Diego CA 92093

Harvard University
ATTN: Prof. A. Dziewonski
Hoffman Laboratory
Department of Earth, Atmospheric & Planetary
Sciences
20 Oxford Street
Cambridge MA 02138

Boston College
ATTN: Prof. J. Ebel & Prof. A. Kafka
Department of Geology & Geophysics
Chestnut Hill MA 02167

Mission Research Corporation
ATTN: Dr. M. Fisk & Dr. W. Wortman
8560 Cinderbed Rd., Suite 700
Newington VA 22122

Southern Methodist University
ATTN: Dr. Henry Gray
Department of Statistical Science
P.O. Box 750302
Dallas TX 75275-0302

Pacific Northwest National Laboratories
ATTN: Dr. D.N. Hagedorn
P.O. Box 999, MS K5-12
Richland WA 99352

Lawrence Livermore National Laboratory
ATTN: Dr. J. Zucca
P.O. Box 808, L-205
Livermore CA 94551

MIT ERL E34-404
ATTN: Dr. David Harkrider
42 Carlton St.
Cambridge MA 02142-1324

New Mexico State University
ATTN: Prof. Thomas Hearn & Prof. James Ni
Department of Physics, 3D
Las Cruces NM 88003

California Institute of Technology
ATTN: Dr. Donald Helmberger
Division of Geological & Planetary Sciences
Seismological Laboratory
Pasadena CA 91125

Southern Methodist University
ATTN: Dr. E. Herrin & Dr. B. Stump
Department of Geological Sciences
P.O. Box 750395
Dallas TX 75275-0395

Sandia National Laboratories
ATTN: Mr. Pres Herrington
P.O. Box 5800, MS 0975
Albuquerque NM 87185-0975

St. Louis University ATTN: Prof. R. Herrmann & Prof. B. Mitchell Department of Earth & Atmospheric Sciences 3507 Laclede Ave. St. Louis MO 63103	US Geological Survey ATTN: Dr. John Filson 12201 Sunrise Valley Dr., MS-905 Reston VA 22092
University of California, Berkeley ATTN: Prof. L.R. Johnson & Prof. T. McEvilly Earth Sciences Division LBNL 90-2106, MS 90-1116 479 McCone Hall Berkeley CA 94720	Weston Geophysical Corp. ATTN: Mr. James Lewkowicz 57 Bedford St., Ste 102 Lexington MA 02420
Massachusetts Institute of Technology ATTN: Prof. T.H. Jordan Department of Earth, Atmospheric, & Planetary Sciences 77 Massachusetts Ave., 654-918 Cambridge MA 02139	Georgia Institute of Technology ATTN: Prof. L. Long School of Geophysical Sciences Atlanta GA 30332
Massachusetts Institute of Technology ATTN: Dr. R. LaCross, M-200B Lincoln Laboratory P.O. Box 73 Lexington MA 02173-0073	Southern Methodist University ATTN: Dr. G. McCartor Department of Physics P.O. Box 750175 Dallas TX 75275-0175
University of Illinois, Urbana-Champaign ATTN: Prof. F.K. Lamb & Prof. J. Sullivan Department of Physics 1110 West Green Street Urbana IL 61801	US Geological Survey ATTN: Dr. A. McGarr National Earthquake Center 345 Middlefield Rd., MS-977 Menlo Park CA 94025
Oklahoma Geological Survey Observatory ATTN: Dr. J. Lawson, Chief Geophysicist Number One Observatory Lane P.O. Box 8 Leonard OK 74043-0008	Office of the Secretary of Defense DDR&E Washington DC 20330
University of California, Santa Cruz ATTN: Dr. T. Lay, Dr. S. Schwartz, & Dr. R. Wu Institute of Tectonics, Earth Sciences Dept. A232 Earth & Marine Sciences Building Santa Cruz CA 95064	Yale University ATTN: Prof. J. Park Department of Geology & Geophysics P.O. Box 208109 New Haven CT 06520-8109
	University of Cambridge ATTN: Prof. Keith Priestly Bullard Lab, Department of Earth Sciences Madingley Rise, Madingley Road Cambridge CB3 OEZ UNITED KINGDOM

BBN Systems & Technologies
ATTN: Dr. J.J. Pulli
1300 N. 17th St., Suite 1200
Arlington VA 22209

DTR Associates/Weston Geophysical
ATTN: Dr. Delaine Reiter
325 West Main Street
Northborough MA 01532

Columbia University
ATTN: Prof. P. Richards & Dr. J. Xie
Lamont-Doherty Earth Observatory
61 Route 9W
Palisades NY 10964

Woodward-Clyde Federal Services
ATTN: Dr. C.K. Saikia
566 El Dorado Street, Suite 100
Pasadena CA 91101-2560

University of Southern California, Los Angeles
ATTN: Prof. C.G. Sammis
Center for Earth Sciences
University Park
Los Angeles CA 90089

**Secretary of the Air Force
(SAFRD)**
Washington DC 20330

University of California, Davis
ATTN: Dr. R. Shumway
Division of Statistics
1 Shields Ave.
Davis CA 95616-8671

AFOSR/NL
110 Duncan Avenue, Suite B115
Bolling AFB
Washington DC 20332-0001

Los Alamos National Laboratory
ATTN: Dr. H. Patton, Dr. S.R. Taylor,
Dr. C.L. Edwards, Dr. D.C. Pearson, &
Dr. Scott Phillips
P.O. Box 1663, MS D408
Los Alamos NM 87545

Massachusetts Institute of Technology
ATTN: Prof. M.N. Toksoz
Earth Resources Lab, 34-440
42 Carleton Street
Cambridge MA 02142

WINPACC/CA/FO
ATTN: Dr. L. Turnbull
New Headquarters Bldg., Room 4W03
Washington DC 20505

National Science Foundation
ATTN: Dr. Daniel Weill
Division of Earth Sciences, EAR-785
4201 Wilson Blvd., Room 785
Arlington VA 22230

NTNF/NORSAR
ATTN: Dr. Svein Mykkeltveit
Granaveien 33
P.O. Box 51
N-2007 Kjeller
NORWAY

Australian Geological Survey Organization
ATTN: Dr. David Jepsen
Cnr. Jerragomerra Ave. & Nindmarsh Dr.
Canberra, ACT 2609
AUSTRALIA

Atomic Weapons Establishment
ATTN: Dr. P. Marshall, Dr. David Bowers, &
Dr. Alan Douglas
Blacknest, Brimpton
Reading RG7 4RS
UNITED KINGDOM

**University of Bergen
ATTN: Prof. Eystein Husebye
Institute for Solid Earth Physics, IFJ
Allegaten 41
N-5007, Bergen
NORWAY**

**AFTAC/CA(STINFO)/TT/TTD/TTE/TTR
1030 South Highway A1A
Patrick AFB FL 32925-3002**

(This page intentionally left blank.)

APPENDIX

To: Distribution

From: Bob Blandford

Subject: Correlation for 23July99 Shuttle Event at DLIAR

Date: 04 November, 1999

- (1) Figure 1 shows the ~06:53 event, with an apparent duration of about 10 minutes, filtered 0.2 to 5 Hz with about 45 minutes of noise preceding. Figure 2 shows the same traces but filtered 0.8 to 1.2 Hz.

We note that there is a substantial amount of noise on channel DLI02, especially just before arrival of the signal. The quietest channel appears to be channel DLI04.

Figure 3 shows channel DLI04 in 5 passbands plus a raw trace. We see that the best S/N is found at 1 Hz and 2 Hz. At 0.5 Hz the S/N is fair and at 0.25 Hz the S/N is very poor, as was also seen in analysis of the 20/08/98 event at Warramunga in my memo of 02 November.

This event differs from the Warramunga event in that the S/N is much better at 2 and 4 Hz; even though the signal has travelled about 2500 km. This was not found for the Tanana event at Palmyra; however this could be because the large aperture pipe arrays likely used in that deployment filtered out the higher frequencies in the signals.

- (2) The coordinates of the array elements are as follows:

	LAT	LONG
DLI01	35.8741	-106.3325
DLI02	35.8636	-106.3254
DLI03	35.8655	-106.3401
DLI04	35.8676	-106.3342

DLI04 is the central element; DLI01 is to the N, DLI02 to the SE, and DLI03 to the SW.

Correlation analysis of a 260 second window centered on the peak signal reveals that the signal arrives on channels 01 and 04 within 0.1 seconds of each other; so that the back azimuth may be calculated as within a degree of the true back azimuth to Cape Canaveral.

- (3) The table below gives the correlation results for 260-second windows filtered through bandpasses centered at 1 second period and 0.5 seconds period (0.8-1.2 and 1.6-2.4 Hz respectively). The amplitudes for the 2 Hz cross-correlations were measured at the same delays determined for the maxima for the 1 Hz cross-correlations. This ensures that correlation amplitudes were measured at the offsets suitable for beamforming and not at random maxima; which is a risk for low S/N.

Inter d(km) val		relative azimuth degrees	Observed r		Theoretical r	
			1.sec	.5sec	1.sec	.5sec
			1.Hz	2.Hz	1.Hz	2.Hz
04-01	0.73	90	.69	.32	.72	.17#
04-02	1.04	14	.84	.42	.81	.39
04-03	0.58	34	.84	.67	.91#	.67
03-01	1.17	65	.63	.10	.46#	.14
03-02	1.49	20	.76	.25	.60#	.06#
02-01	1.41	44	.53	.14	.46	.05

lies outside 95% confidence interval on observed r

The confidence intervals on observed r were calculated using the Fisher r to z transform with 208 degrees of freedom for 1 seconds period, and 416 dof for 0.5 seconds period. The dof are given by $2BT$, where B is the bandwidth and T is the time window for correlation. For both periods, T is 260 seconds; B is 0.4 seconds (0.8 to 1.2 Hz) for 2 second period and 0.8 seconds (1.6 to 2.4 Hz) for 0.5 second period.

These correlation estimates were corrected for noise as was done in Blandford (1998) for the Tanana signal. In general the corrections were modest but significant; for example the correction at 1.0 second period, for the distance interval between sensors 03 and 02, increased the correlation estimate from 0.58 to 0.76. Before the correction, the correlation would have been in agreement with the MF theory; afterward the MF estimate of 0.60 lay outside the 95% confidence of 0.70 to 0.81 for the estimated observed value of 0.76.

The noise corrections were performed by calculating the mean square noise in a representative time period near the signal, and then subtracting that value from the trace signal autocorrelations. These corrected autocorrelations were then used to calculate the denominator in correlation estimates. Corrections ranged from

5% to 40%.

- (4) Note in the table that the MF theory for squared coherence ("gamma-squared", which they refer to simply as "coherence") leads to theoretical correlation estimates (square root of the squared coherence) between elements which exceed the 95% confidence bounds on the low side in four cases; and on the high side in one case. I have been unable to detect any pattern in these results with respect to direction of propagation. Perhaps one cause of the failure of theory to fit within the data's confidence bounds is additional variance introduced by the noise correction procedure.

Overall, the results of this analysis strongly suggest to me that the MF parameterization is suitable for signals of interest for monitoring.

In addition, the good S/N in this signal, at 2 Hz and even at 4 Hz, suggests that the maximum aperture of the infrasound arrays should be 1 km and, that even for such arrays, there should be additional elements at shorter spacings; perhaps a few 100 meters.

The 4 Hz signal with good S/N at 2500 km also suggests that a sampling rate greater than 10 sps would be desirable.

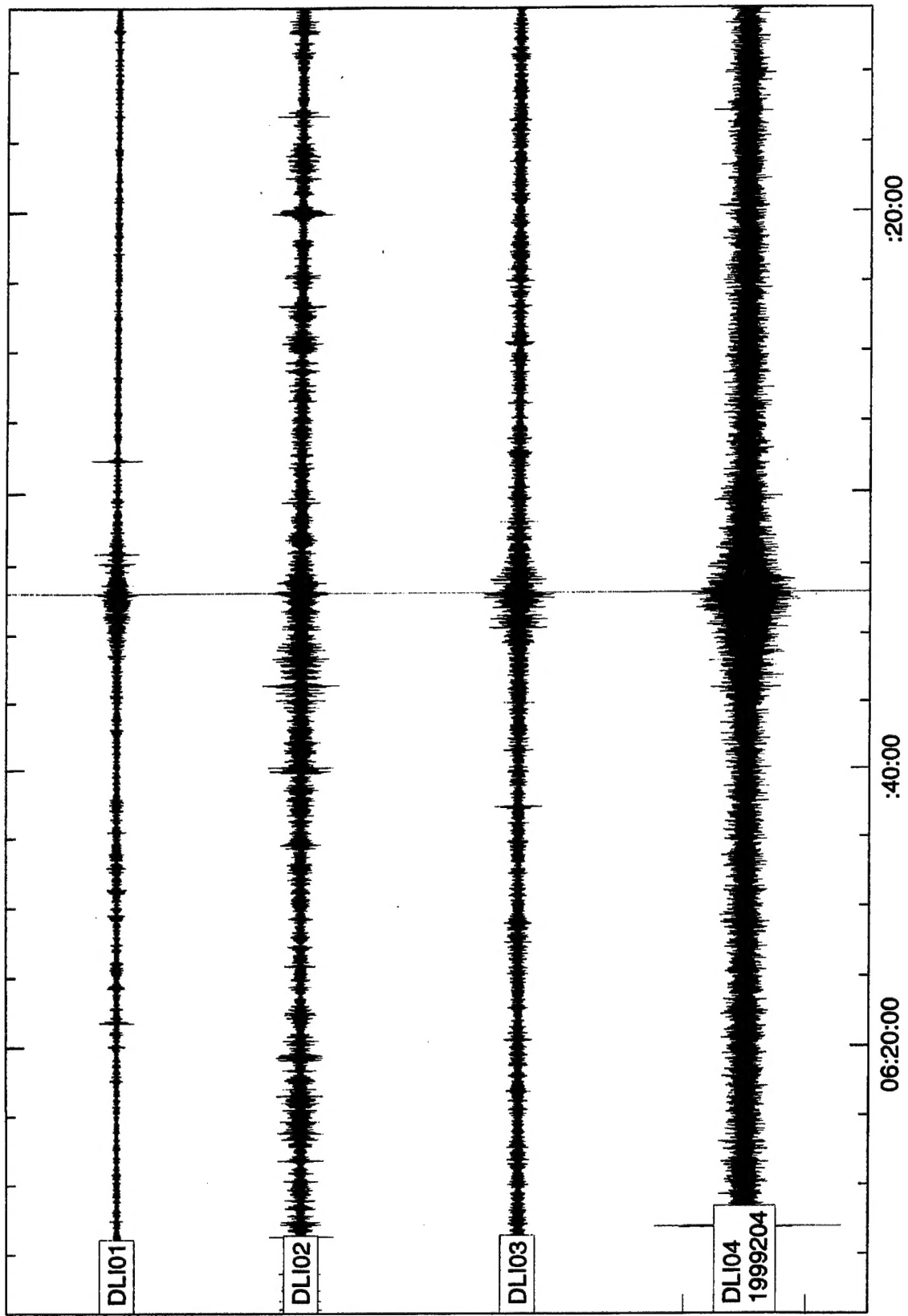
A previous study (Blandford, 1998) based on data from the nuclear test Tanana, also suggested that the MF theory is appropriate, and suggested that the optimum aperture of such an array is 1 km, or perhaps even smaller.

The same conclusion was reached in analysis of the 20/08/98 Warramunga event discussed in my 02 November memo.

- (5) A summary of this memo is that analysis of several events; including two events for which data recently became available, supports the conclusion that the optimum infrasound array aperture is 1 km.

A next step would be to analyze the Shuttle data from Lac du Bonnet. The S/N there appears to be somewhat higher than at DLIAR, and the sampling rate is 20 sps, so that higher frequencies may be detected.

Shuttle Signal at DLIAR, July 23, 1999, 0.2 Hz HP

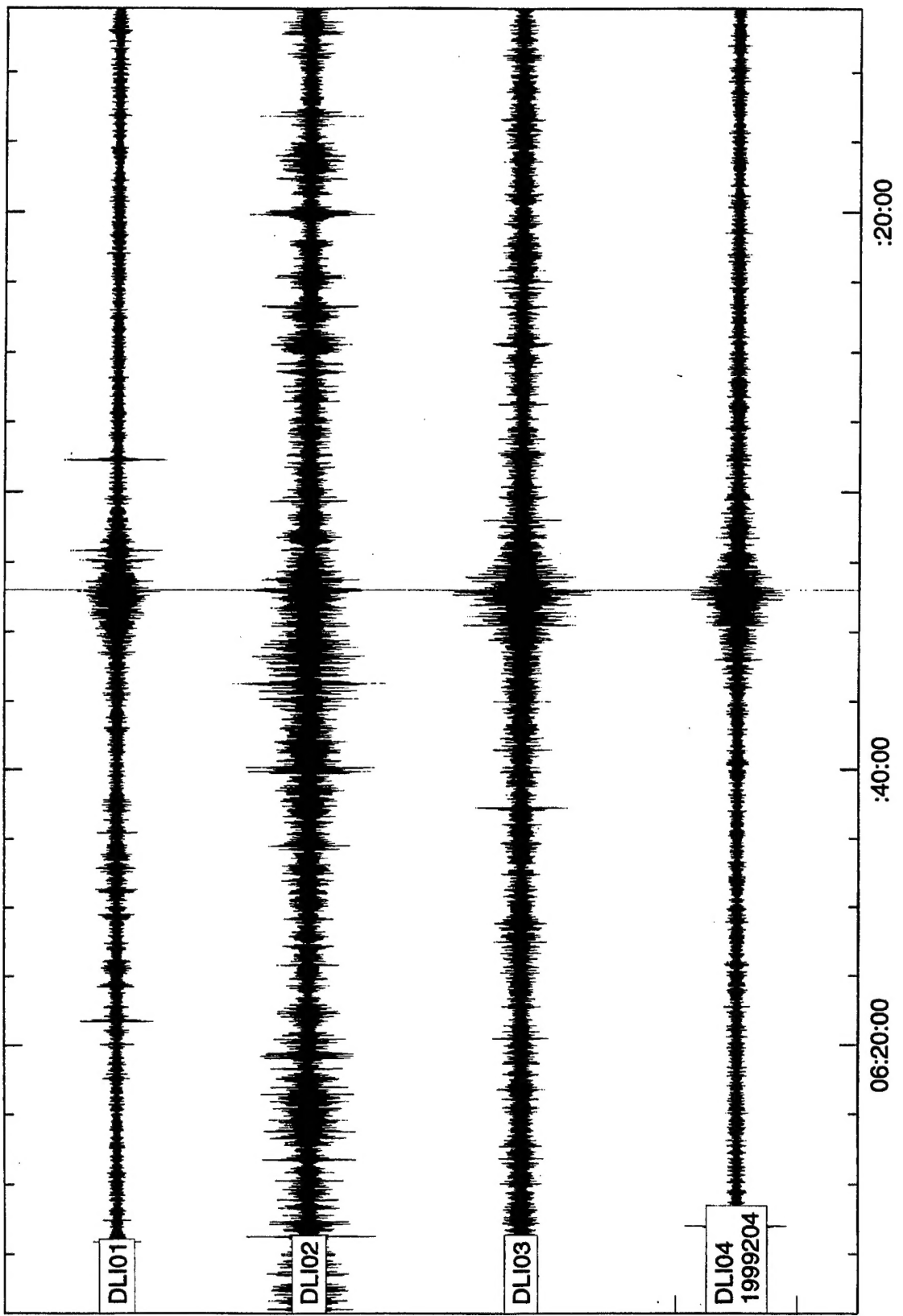


True Relative Amplitude, No Gain Corrections

Time: hr:min:sec, Signal Max at ~06:53

Figure A-1. Shuttle Signal at DLIAR, 23 July 1999, 0.2 Hz HP

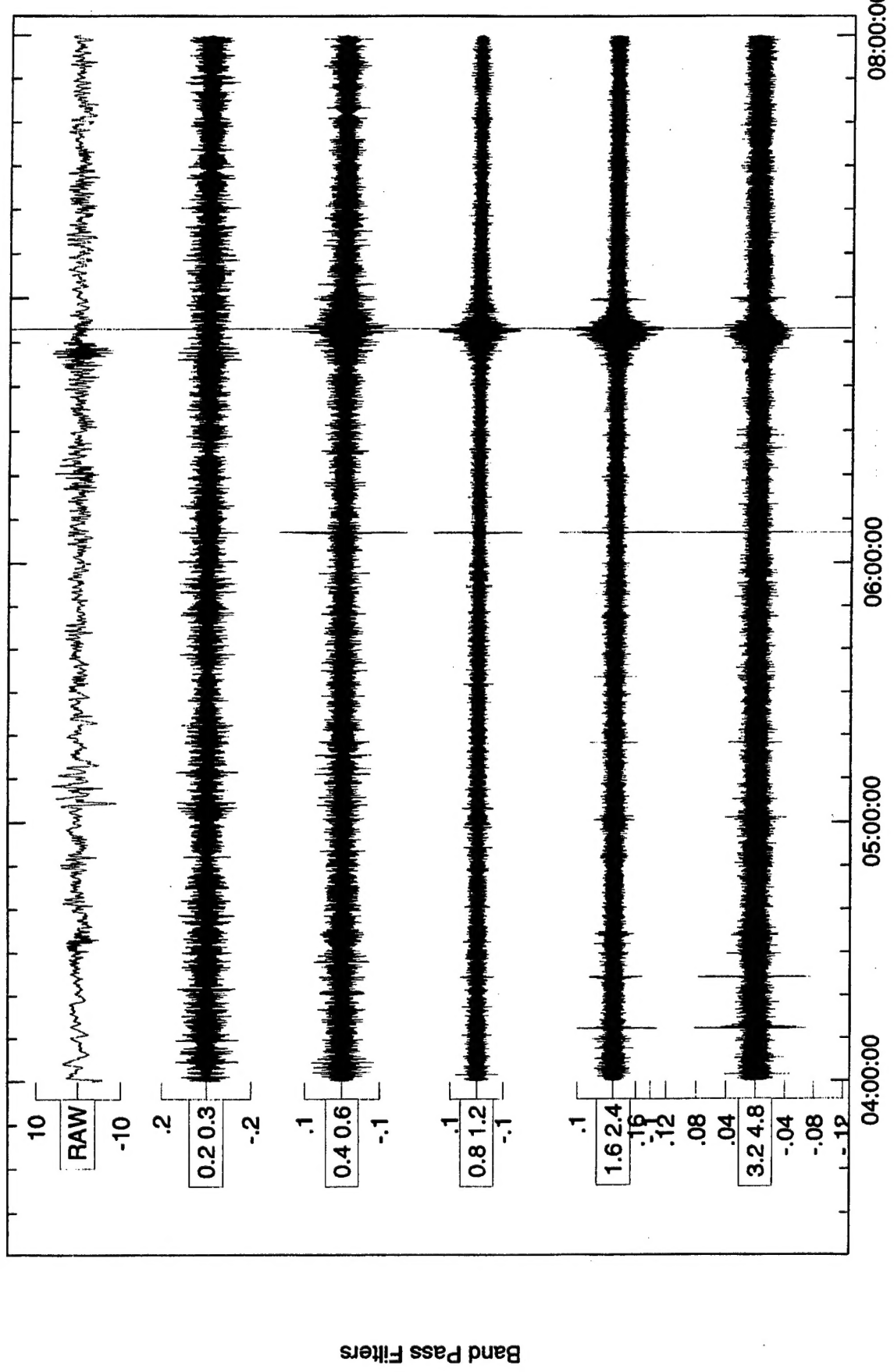
Shuttle Signal at DLIAR, July 23, 1999, 0.8-1.2 BP



True Relative Amplitude, No Gain Corrections

Figure A-2. Shuttle Signal at DLIAR, 23 July 1999, 0.8 - 1.2 BP

Shuttle Signal at DL104, July 23, 1999



Time: hr:min:sec, Signal Max at ~06:53

Figure A-3. Shuttle Signal at DL104, 23 July 1999

Band Pass Filters